Late Neoarchean subduction-related crustal growth in the Northern Liaoning region of the North China Craton: Evidence from ~2.55-2.50 Ga granitoid gneisses

Wei Wang, Shuwen Liu, Peter A. Cawood, Xiang Bai, Rongrong Guo, Boran Guo, Kang Wang

PII: S0301-9268(16)30162-0
DOI: http://dx.doi.org/10.1016/j.precamres.2016.05.018
Reference: PRECAM 4519

To appear in: *Precambrian Research*

Received Date: 16 February 2016
Revised Date: 13 May 2016
Accepted Date: 22 May 2016

Please cite this article as: W. Wang, S. Liu, P.A. Cawood, X. Bai, R. Guo, B. Guo, K. Wang, Late Neoarchean subduction-related crustal growth in the Northern Liaoning region of the North China Craton: Evidence from ~2.55-2.50 Ga granitoid gneisses, *Precambrian Research* (2016), doi: http://dx.doi.org/10.1016/j.precamres.2016.05.018

Late Neoarchean subduction-related crustal growth in the Northern Liaoning region of the North China Craton: Evidence from ~2.55-2.50 Ga granitoid gneisses

Wei Wang[a,b,c], Shuwen Liu[b,*], Peter A. Cawood[c], Xiang Bai[d], Rongrong Guo[e], Boran Guo[b], Kang Wang[b]

[a] The State Key Laboratory of Geological Processes and Mineral Resources, School of Earth Sciences and Resources, China University of Geosciences, Beijing 100083, PR China

[b] The Key Laboratory of Orogenic Belts and Crustal Evolution, Ministry of Education, School of Earth and Space Sciences, Peking University, Beijing 100871, PR China

[c] Department of Earth and Environmental Sciences, University of St Andrews, St Andrews KY16 9AL, UK

[d] Institute of geology, China Earthquake Administration, Beijing 100029, PR China

[e] College of Resources and Civil Engineering, Northeastern University, Shenyang 110819, PR China

Corresponding author:

Shuwen Liu

School of Earth and Space Sciences, Peking University, Beijing 100871, China

Tel: 86-10-62754163; Fax: 86-10-62754163

Email: swliu@pku.edu.cn

Abstract The North China Craton (NCC), dominated by ~2.6-2.5 Ga tectonothermal events, provides a natural laboratory to study Neoarchean crustal growth and geodynamic evolution. Late Neoarchean granitoid gneisses are well exposed in the Northern Liaoning Province, located north of the ancient Anshan-Benxi terrane along the northeastern margin of the Eastern Block (EB) of the NCC. LA-ICPMS zircon U-Pb isotopic dating reveal that granitoid gneisses in the Qingyuan area can be grouped into two major episodes, i.e., ~2559-2534 Ma strongly gneissic quartz dioritic and tonalitic to trondhjemitic gneisses; and ~2529-2495 Ma weakly gneissic to massive quartz monzodioritic and monzogranitic gneisses, with subordinate tonalitic to trondhjemitic gneisses. The late magmatic episode was accompanied by regionally high-grade metamorphism (~2510-2495 Ma). Most granitoid gneisses display highly depleted zircon $\varepsilon Hf(t_2)$ values (+4.2-+8.1), whereas one monzogranitic gneiss shows negative values of -4.7 to -1.0, indicating late Neoarchean crustal growth with minor involvement of ancient continental materials probably sourced from the Anshan-Benxi terrane.

Geochemical and petrogenetic studies reveal that the quartz dioritic magmas were derived from partial melting of plagioclase-poor garnet amphibolites or eclogites metamorphosed from oceanic slab materials, with slab melts contaminated by mantle wedge peridotites during ascent. The tonalitic to trondhjemitic magmas stemmed from partial melting of mainly juvenile metabasaltic rocks with minor metagreywackes of lower arc crust. In comparison, the quartz monzodioritic and monzogranitic magmas were derived respectively from partial melting of depleted mantle sources metasomatized by slab-derived fluids and metagreywackes with different crustal resident ages at middle to lower crustal levels.

Combined with previous studies of metavolcanic rocks, the Northern Liaoning Province

records late Neoarchean crustal growth, evolving from mid-ocean ridge, through initiation and maturation of an intra-oceanic arc, to arc-continent collision. Arc-continent accretion and possibly slab rollback processes may have triggered reworking of both juvenile arc crust and minor ancient continental margin materials, generating the magmatic precursors for the monzogranitic gneisses. Overall, the intense late Neoarchean crustal growth of the EB was controlled mainly by arc-continent accretion, possibly linked to global assembly of cratonic fragments.

Keywords: Late Neoarchean granitoid gneisses; Crustal growth; Intra-oceanic arc and arc-continent accretion; Northern Liaoning Province; Northern margin of North China Craton

1. Introduction

When and how the continental crust formed, evolved, and preserved, as well as crust-mantle geodynamic regimes, are key research issues (Condie, 1998; Hawkesworth et al., 2009, 2010; Dhuime et al., 2011; Cawood et al., 2013; Condie and Kröner, 2013; Spencer et al., 2015). During the Hadean to Paleoarchean, komatiites and tholeiitic basalts, with some felsic rocks and/or anorthosites, constitute the major crustal components. Geochemical and thermodynamic modellings suggest plume- or delamination-driven geodynamics (Kawai et al., 2009; Johnson et al., 2013; Griffin et al., 2014; Reimink et al., 2014). Mantle cooling and crustal thickening led to fundamental changes in crust formation regimes after ~3.2-3.0 Ga, possibly marking the onset of plate tectonics (Cawood et al., 2006; Herzburg et al., 2010; Dhuime et al., 2012, 2015). Though early plate tectonics are considered as hot subduction processes with frequent slab breakoff, subduction-accretion processes may have played crucial roles during the Neoarchean, reflected by Meso- to Neoarchean eclogites, pervasive K-rich granitoid magmatism, and rapid decrease in komatiite production (O'Neil et al., 2007; Condie and O'Neill, 2010; Wan et al., 2012, 2015; Mints et al., 2014).

The North China Craton (NCC) is dominated by late Neoarchean (~2.6-2.5 Ga) tectonothermal events, especially in its Eastern Block (EB) (Fig. 1A; Liu et al., 2002, 2004; Zhao et al., 2005, 2012; Zhai and Santosh, 2011, 2013; Wan et al., 2014). Models of Neoarchean crustal development of the NCC include mantle plume and magmatic arc settings. The former model has been invoked on the basis of voluminous granitoid gneisses, counterclockwise metamorphic P-T-t paths of mafic granulites and ~2.7 Ga komatiites preserved in Western Shandong (Zhao et al., 1998, 2005; Geng et al., 2006, 2012; Liu et al.,

2013; Wu et al., 2013a, 2014). In contrast, others favor the micro-continent accretion processes, with late Neoarchean suprasubduction zone ophiolites, arc-trench systems, and related tectonothermal events (Zhai and Santosh, 2011, 2013; Li et al., 2015; Santosh, 2015; Tang et al., 2015, 2016). Recently, a late Neoarchean intra-oceanic arc system stretching over 1000 km has been proposed along the northwestern EB, which is distinct from the interior EB in that it records ~2.6-2.5 Ga crustal growth but with only very limited involvement and reworking of ≥ 2.7 Ga basement rocks (Fig. 1B; Liu et al., 2002, 2004, 2008, 2011; Wang et al., 2004, 2015a; Guo et al., 2013, 2015a; Bai et al., 2014a,b, 2015, 2016; Wu et al., 2014). Within this large arc system, the Northern Liaoning Province (NLP) in the eastern segment of the northern margin of the NCC have received less study apart from some geochronological and geochemical data on the constituent rock units (Figs. 1A and 2; e.g., Wan et al., 2005a,b; Bai et al., 2014b; Wu et al., 2016). The province is bounded to the east by ~2.7 Ga crystalline basement (Guo et al., 2015b) and to the south by the Anshan-Benxi terrane, and provides an opportunity to study late Neoarchean crustal growth and reworking (Fig. 1; Song et al., 1996; Wan et al., 2013).

In this study, new geological, petrological, zircon U–Pb and Lu–Hf isotopic and whole-rock geochemical data are reported for late Neoarchean granitoid gneisses in the Qingyuan area of the NLP with the aim of: (1) establishing the lithological assemblages and geochronological framework; and (2) deciphering their petrogenesis and Neoarchean tectonic implications. These data will then be integrated with our recent studies along the northern margin of the EB, as well as previous studies of the Anshan-Benxi terrane, to propose a model for crustal growth and crust-mantle geodynamic mechanisms of the NLP and EB.

2. Geological background

The North China Craton is one of the oldest cratons in the world, with ~3.8 Ga rocks identified from Anshan area in the Eastern Liaoning Province (Fig. 1; Liu et al., 1992, 2008; Song et al., 1996; Wan et al., 2009). The craton consists of an Eastern Block (EB) and a Western Block (WB), which were amalgamated along the intervening N-S trending Trans-North China Orogen (TNCO) at ~1.85 Ga (Zhao et al., 1998, 2005, 2012; Guo et al., 2002, 2005; Liu et al., 2006, 2012, 2014). The WB was formed by collision between the Yinshan Block in the north and the Ordos Block in the south along the E-W trending Inner-Mongolia suture zone (IMSZ, or "Khondalite Belt") at ~1.95 Ga. The EB experienced Paleoproterozoic rifting and subsequent subduction–collision processes, forming the Jiao-Liao-Ji Belt (Luo et al., 2004; Li and Zhao, 2007; Santosh et al., 2007a,b; Guo et al., 2012). After final amalgamation, the NCC records multiple Paleo- to Mesoproterozoic extension-related tectonothermal events in response to the prolonged Columbia/Nuna breakup (Zhao et al., 2004; Peng et al., 2008; Wang et al., 2013a, 2015b,c; Zhai et al., 2015).

The NLP is located to the north of the Anshan-Benxi terrane (ABT), and dominated by Neoarchean granitoid gneisses and supracrustal sequences termed the Qingyuan granite-greenstone belt (Fig. 1; Zhai et al., 1985; Peng et al., 2015). Trondhjemitic gneisses dated at ~3.80 Ga, occur at several localities in east Anshan, and a ~4.17 Ga xenocrystic zircon grain is reported in the Benxi area (Song et al., 1996; Wan et al., 2009, 2012, 2013; Cui et al., 2013). Zircon Lu-Hf and O isotopic data of these units indicate both crustal growth and reworking at ~3.8 Ga (Song et al., 1996; Liu et al., 2008; Wang et al., 2015d). These Eoarchean rocks are enveloped mainly by ~3.45-2.90 Ga trondhjemitic gneisses and granites,

which were overprinted by Neoarchean tectonothermal events (Wan et al., 2012, 2013, 2015).

Based on hornblende $^{40}Ar/^{39}Ar$ isotopic and whole-rock Sm-Nd isotopic dating data, the NLP was initially divided into the Neoarchean Hunbei granite-greenstone belt and the Mesoarchean Hunnan high-grade gneissic terrane that are separated by the Hunhe Fault (Fig. 2A; Wang et al., 1987; Li and Shen, 2000). Recent field geology and zircon U-Pb isotopic dating data reveal that both these two units are dominated by late Neoarchean Tonalite-Trondhjemite-Granodiorite (TTG) gneisses and supracrustal volcano-sedimentary sequences that were subjected to amphibolite to granulite facies metamorphism (Wan et al., 2005a,b). The supracrustal sequences occupy ~20% of the exposed basement rocks in the NLP, and outcrop chiefly in the Tangtu, Dasuhe, Sandaoguan, Hongtoushan and northern Qingyuan areas, which are well-known for the development of massive sulfide Cu-Zn deposits (Fig. 2A; Wan et al., 2005a; Zhu et al., 2015). The supracrustal sequences are subdivided into three units, i.e., the Shipengzi, Hongtoushan and Nantianmen formations from the base upwards. These supracrustal rocks occur as intercalated successions or xenoliths in the granitoid gneisses, and consist mainly of hornblende two pyroxene granulites, (pyroxene) amphibolites, fine-grained biotite plagioclase gneisses, sillimanite biotite gneisses, banded iron formations (BIFs), and marbles (Zhai et al., 1985). Bai et al. (2014b) recognized mafic volcanism of >2571 Ma and ~2530 Ma, in the Tangtu-Majuanzi area, with the early episode also recorded in the Hongtoushan area (Zhu et al., 2015). ~2600 Ma amphibolites are recently detected in the Dasuhe area based on our unpublished chronological data. Protoliths of these metavolcanic rocks are tholeiitic basalts, andesites, dacites, and pyroclastic rocks, likely formed within an arc setting (Wan et al., 2005b).

Intrusive granitoid gneisses are the dominant lithologies in the NLP, and they consist chiefly of dioritic and TTG gneisses as well as potassium-rich granitoid rocks comprising monzodioritic, granodioritic and monzogranitic gneisses (Wan et al., 2005a). Charnockitic gneisses are locally preserved in the Xianjinchang and Dasuhe areas. The protoliths of the voluminous TTG and less dioritic gneisses formed at 2571-2518 Ma, whereas monzodiorites, granodiorites, and monzogranites were emplaced at ~2522-2496 Ma coeval with regional ~2510-2470 Ma amphibolite to granulite facies metamorphism (Wan et al., 2005a; Grant et al., 2009; Bai et al., 2014b; Peng et al., 2015). These later potassium-rich lithologies outcrop chiefly in the Shiwenchang, Sandaoguan, Hongmiaozi, Dasuhe, and Huiyuan areas, as well as some to the north of the Nanzamu and Qingyuan areas (this study; Fig. 2A). Previous studies on the metamorphism revealed that garnet amphibolites to the north of Hunhe Fault record peak metamorphic P-T conditions of 780-810 □ and 7.65-8.40 kbar, suggesting a granulite facies metamorphic condition (Wu et al., 2013b). Granulites was also locally detected in Xianjinchang and Dasuhe areas (Fig. 2; Wan et al., 2005a; Wu et al., 2016). Nonetheless, the general lack of granulite facies metamorphic mineral associations or featured metamorphic mineral(s) with retrograde metamorphic reaction records for most rocks in the study area, indicates that most basement rocks in the NLP were subjected to generally high-grade amphibolite facies and only locally reached granulite facies metamorphism. The counterclockwise metamorphic P-T-t paths recorded by the mafic granulites and garnet amphibolites in the NLP have been linked to a mantle plume setting (Grant et al., 2009; Wu et al., 2013b). However, Peng et al. (2015) suggested metamorphism was a response to mantle wedge-absent flat-"hot" subduction.

Precambrian basement rocks within the Eastern Block are unconformably overlain by Mesozoic volcano-sedimentary rocks, and intruded by late Paleozoic to Mesozoic plutonic granitoids (Fig. 2A). They may represent responses to orogenic processes in the Central Asian Orogenic Belt and later lithospheric thinning in Eastern China (Zhang et al., 2012, 2014).

3. Geology and petrology of Neoarchean granitoid gneisses in the Qingyuan area

In the Qingyuan area, metamorphosed supracrustal rocks crop out in the Xianjinchang, Xiajiabao, and Hongtoushan areas (Fig. 2B), and consist chiefly of mafic granulites, (garnet) amphibolites, hornblende plagioclase gneisses, and biotite plagioclase gneisses, intercalated with some banded iron formations (BIFs) and sillimanite biotite gneisses (Fig. 3A; Wan et al., 2005a,b; Zhu et al., 2015). Metamorphosed plutonic granitoid gneisses are subdivided into two groups, i.e., sodium-rich group consisting of quartz dioritic and TTG gneisses, and potassium-rich group comprising quartz monzodioritic and monzogranitic rocks. Tonalitic and trondhjemitic gneisses are the dominant granitoid gneisses (Fig. 3B-D). They are generally deformed with strong gneissosity, but in local low strain domains an intrusive relationship is preserved with the supracrustal rocks as confirmed by the preservation of metavolcanic xenoliths ranging in size from centimeters to meters (Fig. 3C-D). In comparison, the subordinate quartz monzodioritic and monzogranitic gneisses show weakly gneissic to massive structures (Fig. 3E-H). Of which, the monzogranitic gneiss samples are mainly distributed at two localities, i.e., some to the north of the Nanzamu town extending discontinuously from north to south for ~15 km, and others sporadically adjacent to the Xianjinchang and Qingyuan areas (Fig. 2B and Supplementary Table 1). Similarly, quartz

monzodioritic gneisses outcrop locally at Xianjinchang-Dasuhe and Nanzamu areas. Locally, monzogranitic veins crosscut tonalitic gneisses, together with the occurrence of supracrustal xenoliths within quartz monzodioritic gneisses (Fig. 3E-F), indicating that these potassium-rich granitoid gneisses represent the latest Neoarchean tectonomagmatic events.

A total of twenty-six samples of representative granitoid gneisses were collected from the Qingyuan area, including two quartz dioritic gneisses, fifteen tonalitic and trondhjemitic gneisses, three quartz monzodioritic gneisses, and six monzogranitic gneisses (Figs. 2B and 4, and Supplementary Table 1). The quartz dioritic gneisses show medium- to coarse-grained textures and gneissic structures, with a major mineral association of plagioclase (52-55%), hornblende (12-18%), K-feldspar (10-12%), quartz (6-12%), and biotite (6-8%), and accessory minerals of zircon, apatite, epidote, and zoisite (Fig. 4A). Mafic minerals were partially altered to chlorite, whereas feldspar crystals were commonly subjected to sericitization and kaolinitization. Most TTG gneisses display gneissic structures and medium- to coarse-grained textures (Fig. 4B-D). Though minor TTG gneisses show fine- to medium-grained textures, the presence of amphibolite xenoliths and absence of local interlayering with mafic to andesitic metavolcanic rocks suggest that their magmatic precursors should be plutonic granitoids rather than felsic volcanic rocks (Fig. 3B-D). The tonalitic gneisses are mostly biotite plagioclase gneisses, and are composed of plagioclase (48-52%), quartz (25-28%), biotite (9-15%), and K-feldspar (7-12%) (Fig. 4B) with accessory zircon, apatite, and zoisite. Some tonalitic gneisses were subjected to granulite-facies metamorphism, and show mineral assemblages of plagioclase (52-54%), quartz (22-25%), clinopyroxene (5-9%), orthopyroxene (7-9%), hornblende (6-8%), and minor K-feldspar with accessory minerals of magnetite,

apatite, and zircon (Fig. 4C). Trondhjemitic gneisses consist mainly of plagioclase (54-56%), quartz (28-32%), K-feldspar (4-8%) and mafic minerals (biotite+hornblende of 5-8%) (Fig. 4D). Zircon, apatite, and zoisite are the dominant accessory minerals. The quartz monzodioritic gneisses show medium-grained textures and weakly gneissic structures, and most of them consist of plagioclase (36-42%), K-feldspar (16-22%), orthopyroxene (8-12%), hornblende (6-10%), quartz (6-10%), clinopyroxene (5-8%), and biotite (3-5%) (Fig. 4E), with accessory zircon, magnetite and apatite. The monzogranitic gneisses display medium- to coarse-grained textures and weakly gneissic to massive structures. Their mineral assemblages are plagioclase (36-42%), K-feldspar (26-28%), quartz (28-33%) and minor amount of biotite with zircon, magnetite and zoisite as the accessory minerals (Fig. 4F).

4. Analytical procedures

Whole-rock samples were trimmed to remove the weathered surfaces, and the fresh portions were then chipped and powdered in an agate mill to about 200 mesh to prepare for analyzing for major and trace elements. Major elements were analyzed using X-ray Fluorescence (XRF, Thermo Arl Advant XP+) at the Key Laboratory of Orogenic Belts and Crustal Evolution, Ministry of Education, School of Earth and Space Sciences, Peking University. Loss on ignition (LOI) values were determined by measuring the weight loss after heating the samples at 1050□. The analytical precision is 0.5% for major element oxides (Liu et al., 2004, 2005; Wang et al., 2012a).

For trace element analyses, the sample powders were pre-treated at the Peking University, as described below. Firstly, the powders were accurately weighted (25 mg) into

Savillex teflon beakers, and placed within a high-pressure bomb with a 1:1 mixture of HF–HNO_3, and heated for 24 hours at 80℃, then evaporated. After evaporation, 1.5 ml HNO_3, 1.5 ml HF and 0.5 ml $HClO_4$ were added, and the beakers were capped for digestion within a high-temperature oven at 180 ℃ for 48 hours or longer until the powders were completely digested. Finally, the residue was diluted with 1% HNO_3 to 50 ml. Trace elements, including rare earth elements (REEs), were measured using an ELEMENT-I plasma mass spectrometer (Finnigan-MAT Ltd.) at the Key Laboratory of Orogenic Belts and Crustal Evolution. The international standards GSR-1 (granite), GSR-9 (diorite), and GSR-14 (granitoid gneiss) were used for analytical control.

Six representative samples, including three trondhjemitic gneisses, one tonalitic gneiss, and two monzogranitic gneisses, were selected for zircon U-Th-Pb and Lu-Hf isotopic analyses (Supplementary Tables 2 and 3). Zircon grains were separated by standard density and magnetic techniques, and then handpicked under a binocular microscope. The separated zircon grains were mounted in epoxy resin discs, and polished to half the grain thickness. Prior to analyses, cathodoluminescence (CL) images were obtained using a scanning electron microscope at the SEM Laboratory of Peking University. Then, they were simultaneously analyzed for zircon U-Pb isotopes and trace elements using a laser ablation inductively coupled plasma mass spectrometer (LA-ICP-MS) at the Geological Lab Center, China University of Geosciences, Beijing (CUGB) (Yuan et al., 2004). During analysis, the laser spot diameter and frequency were 36 μm and 10 Hz, respectively. Harvard zircon 91500 was used as an external standard for zircon U-Th-Pb analyses, and NIST610 as an external standard to calculate the contents of U, Th, Pb, and other trace elements in the analyzed zircon grains.

The $^{207}Pb/^{206}Pb$ and $^{206}Pb/^{238}U$ ratios were calculated using the GLITTER program (van Achterbergh et al., 2001), and common Pb was corrected using the method of Anderson (2002). Age calculations and concordia plots were done using Isoplot (ver. 3.0) (Ludwig, 2003). Zircon Lu-Hf isotopic analyses were performed on the similar internal domains or close to the original pit used for LA-ICPMS U-Pb isotopic dating analyses, using a Neptune Plus MC-ICP-MS (Thermo Fisher Scientific, Gemany) attached to a Geolas 2005 excimer ArF laser ablation system (Lambda physik, Göttingen, Germany) at the state Key Laboratory of Geological Processes and Mineral Resources, China University of Geosciences in Wuhan (see Hu et al. (2012) for details of analytical techniques). For zircon domains that are large enough, analyses for U-Pb and Lu-Hf isotopes were carried out at separate sub-domains as possible. Whereas zircon Lu-Hf isotope analyses for small zircon domains were carried out partly on or entirely overlapping the pits used for U-Pb isotopic dating. Nonetheless, the nearly consistent zircon initial $^{176}Hf/^{177}Hf$ isotopic ratios (calculated at respective apparent $^{207}Pb/^{206}Pb$ ages) for each dated sample suggest that the above analyzed strategies did not compromise their actual Lu-Hf isotopic features (Supplementary Table 3). Beam diameter of 44 μm and repetition rate of 6 Hz were applied, and zircon 91500 and GJ-1 were used as the external standard and the unknown, respectively. During analyses, every eighth analysis of an unknown was followed by analyses of 91500 and GJ-1. The interference of ^{176}Yb and ^{176}Lu on ^{176}Hf could significantly affect the accuracy of obtained $^{176}Hf/^{177}Hf$ ratios. The $^{179}Hf/^{177}Hf$ and $^{173}Yb/^{171}Yb$ ratios were used to calculate the mass bias of Hf (β_{Hf}) and Yb (β_{Yb}), which were normalized to $^{179}Hf/^{177}Hf$ =0.7325 and $^{173}Yb/^{171}Yb$=1.13017 (Segal et al., 2003) using an exponential correction for mass bias. Interference of ^{176}Yb on ^{176}Hf was corrected by

measuring the interference-free ^{173}Yb isotope and using $^{176}Yb/^{173}Yb$ =0.79381 (Segal et al., 2003) to calculate $^{176}Yb/^{177}Hf$. Similarly, the relatively minor interference of ^{176}Lu on ^{176}Hf was corrected by measuring the intensity of the interference-free ^{175}Lu isotope and using the recommended $^{176}Lu/^{175}Lu$ =0.02656 (Blichert-Toft et al., 1997) to calculate $^{176}Lu/^{177}Hf$. We used the mass bias of Yb (β_{Yb}) to calculate the mass fractionation of Lu because of their similar physicochemical properties. The determined $^{176}Hf/^{177}Hf$ ratios for standards 91500 (0.282299±0.000030) and GJ-1 (0.282023±0.000025) are within error of the reported values (Wu et al., 2006).

5. Analytical results

5.1. Whole-rock geochemistry

Geochemical data and calculated parameters of the analyzed twenty-six granitoid gneiss samples are listed in Supplementary Table 1, and are plotted in figures 5-6. Whole-rock geochemical data of several granitoid gneiss samples in the Xinbin area were documented by Peng et al. (2015), which are integrated in the discussions. In the normative An-Ab-Or diagram (Fig. 5A; O'Connor, 1965), nine samples plot in the trondhjemite field, six samples in the tonalite field, and six samples in the granite field. The quartz dioritic (samples 12LN58-1 and 12LN75-2) and quartz monzodioritic gneisses (samples 13LB33-3, 13LB39-1, and 13LB42-5 in this study and eight samples reported by Peng et al. (2015)) also plot in the above diagram, falling into the fields of tonalites and granodiorites, respectively (Fig. 5A). In the K_2O-Na_2O-CaO diagram (Fig. 5B; Moyen et al., 2003), the quartz dioritic, tonalitic, and trondhjemitic gneisses show close affinities to Archean TTG gneisses, constructing a

sodium-rich trend, which are defined here as the DTT series. Whereas the quartz monzodioritic and monzogranitic gneisses with chemical features of potassium-rich granitoids construct a calc-alkaline trend (Barker, 1979), which are defined here as the MM series.

5.1.1. Major element compositions

For the DTT series, the quartz dioritic gneisses show lower SiO_2 contents of 59.14-61.30 wt.%, with MgO contents and Mg# values (100Mg/(Mg+Fe_{total}) atomic ratio) of 0.95-3.37 wt.% and 25.31-49.28, respectively. In comparison, the tonalitic and trondhjemitic gneisses show higher SiO_2 contents (64.23-71.76 wt.%), and have lower MgO contents of 0.52 wt.% to 1.99 wt.% and a larger Mg# value range of 26.62 to 45.30. Granitoid gneisses in the DTT series have K_2O/Na_2O ratios of 0.12-0.62, and belong to the low-K tholeiitic to medium-K calc-alkaline rock series with mostly low K_2O contents of 0.62-1.74 wt.% (Rollinson, 1993; Fig. 5C). The tonalitic gneiss sample 13LB37-3 shows a slightly lower Na_2O content (2.11 wt.%), but also exhibits a lower K_2O/Na_2O ratio of 0.62. Most DTT series samples show moderate A/CNK (molar $Al_2O_3/(CaO+Na_2O+K_2O)$ ratio) values of 0.71-1.07 belonging to metaluminous to weakly peraluminous affinities, except for one tonalitic (12LN72-1) and four trondhjemitic (12LN78-1, 12LN80-2, 13LB47-1, and 13LB47-3) gneiss samples that display strongly peraluminous features with high A/CNK values of 1.17-1.35 (Maniar and Piccoli, 1989). In the MgO versus SiO_2 plot (Fig. 5D), all DTT samples plot in the experimental melt field of metabasalts, but below those of low-silica and high-silica adakites (Martin et al., 2005).

The quartz monzodioritic gneiss samples show SiO_2 contents of 56.84-64.80 wt.% that are comparable with the quartz dioritic gneiss samples, with MgO contents and Mg# values of

1.34-4.52 wt.% and 27.78-51.13, respectively. However, the quartz monzodioritic gneisses are featured by higher K_2O contents (1.84-3.47 wt.%) with dominantly higher K_2O/Na_2O ratios of 0.61-1.11 than those of the DTT series. They all belong to the metaluminous rock series with lower A/CNK values of 0.80-0.99 (Maniar and Piccoli, 1989). The monzogranitic gneiss samples display higher SiO_2 contents of 66.71-74.81 wt.%, and lower MgO contents of 0.62-2.74 wt.% with lower Mg# values of 34.04-48.45, relative to the quartz monzodioritic gneisses. They have the highest K_2O contents of 2.50-4.24 wt.%, with the highest K_2O/Na_2O ratios up to 1.56 (Supplementary Table 1). These monzogranitic gneiss samples show geochemical affinities to metaluminous and peraluminous rock series, with A/CNK values varying from 0.94 to 1.76. In the K_2O versus SiO_2 diagram (Fig. 5C), all MM series samples plot in the field of high-K calc-alkaline rock series. In the MgO versus SiO_2 diagram (Fig. 5D), most quartz monzodioritic gneisses and a monzogranitic gneiss sample 12LN57-2 plot in the fields of low-silica or high-silica adakites. Whereas the other quartz monzodioritic (P10YJD1, P10YJD2, P10YJD3, and P10YJD4) and monzogranitic gneiss samples (12LN59-1, 12LN80-1, 12LN82-2, 12LN83-2, and 13LB31-1) fall in the experimental melt field of metabasaltic rocks (Martin et al., 2005; Peng et al., 2015).

5.1.2. Rare earth elements (REEs)

For the DTT series, quartz dioritic gneiss samples have total rare earth element (TREE) contents of 82-176 ppm, and show moderately differentiated chondrite-normalized REE patterns, yielding $(La/Yb)_N$ and $(Gd/Yb)_N$ ratios of 9.65-23.13 and 2.41-2.97, respectively and weakly negative to positive Eu anomalies (Eu_N/Eu^*_N values of 0.96-1.18) (Fig. 6A; Sun and

McDonough, 1989). In comparison, the tonalitic and trondhjemitic gneiss samples show more variable TREE contents of 17.3-170 ppm, and feature strongly fractionated REE patterns (Fig. 6C), with higher $(La/Yb)_N$ and $(Gd/Yb)_N$ ratios mostly of 9.17-72.29 and 2.12-5.73, respectively, and generally positive Eu anomalies (Eu_N/Eu^*_N values mostly of 1.04-4.80, excepting for samples 12LN61-1 with a lower value of 0.79). The tonalitic gneiss sample 13LB46-5 displays lower $(La/Yb)_N$ and $(Gd/Yb)_N$ values of 5.13 and 1.80, respectively.

With respect to the MM series, quartz monzodioritic gneiss samples display moderately fractionated patterns in the chondrite-normalized REE diagram (Fig. 6E), and show $(La/Yb)_N$ and $(Gd/Yb)_N$ ratios mostly of 9.28-22.59 and 1.47-3.63, respectively, except for sample 13LB33-3 with a lower $(La/Yb)_N$ ratio of 4.72 and a moderate $(Gd/Yb)_N$ ratio of 2.25. They have strongly negative to weakly positive Eu anomalies (Eu_N/Eu^*_N values of 0.53-1.04), with relatively higher TREE contents of 117-494 ppm. Most monzogranitic gneisses have high TREE contents of 37-291 ppm, accompanied by moderate to strongly fractionated chondrite-normalized REE patterns (Fig. 6G). Their $(La/Yb)_N$ and $(Gd/Yb)_N$ ratios range from 6.83 to 98.30 and 2.44 to 8.06, respectively, with moderately negative to positive Eu anomalies (0.69-1.31). However, sample 12LN82-2 (with the highest silica content of 74.81 wt.%) exhibits the lowest TREE content (6.74 ppm) and a concave-upward chondrite-normalized REE pattern (Fig. 6G), with $(La/Yb)_N$ and $(Gd/Yb)_N$ ratios of 16.68 and 2.44, respectively, and a strongly positive Eu anomaly (Eu_N/Eu^*_N value of 4.99).

5.1.3. Other trace elements

On the primitive mantle-normalized multi-element diagrams (Fig. 6B and D), the DTT

series samples display pronounced negative Nb, Ta, Ti and P anomalies and positive Zr and Hf anomalies, and most of them are enriched in Ba, Rb, and K, but depleted in Th. Among these samples, the two quartz dioritic gneiss samples show the highest Sr contents (738-770 ppm) with lower Y (11.3-12.6 ppm) and Yb (1.082-1.404 ppm) contents, corresponding to high Sr/Y ratios of 60.98-65.38 (Fig. 6B). Compared to the quartz dioritic gneisses, the tonalitic and trondhjemitic gneiss samples are characterized by somewhat lower Sr contents of 194-640 ppm and higher Y and Yb contents of 1.48-9.42 ppm and 0.117-1.126 ppm, respectively, yielding Sr/Y ratios of 33.00-314.27 (Fig. 6D). All the DTT series samples have higher Zr/Sm ratios (28.39-107.25) and generally lower Nb/Ta ratios (2.37-18.82, mostly of 5.98-16.83), relative to the chondrite values of 25.29 and 17.57, respectively (Sun and McDonough, 1989).

For the MM series, the quartz monzodioritic gneiss samples are characterized by moderate enrichment of Ba, Zr, and Hf, but strong depletion of Nb, Ta, and Ti, with negative to negligible Sr and P anomalies (Fig. 6F). They have high Sr contents of 341-1209 ppm, together with generally high Y and Yb contents (11.4-42 ppm and 1.17-3.72 ppm, respectively), yielding moderate to high Sr/Y ratios of 9.29-88.33. In comparison to the quartz monzodioritic gneisses, the monzogranitic gneiss samples are enriched in Ba, Rb, K, Zr, and Hf, but are depleted in Nb, Ta, Ti, and P, with negative to positive Sr anomalies (Fig. 6H). They have moderate to high Sr contents of 112-459 ppm, but lower Y (0.622-11.7 ppm) and Yb (0.072-1.316 ppm) contents, corresponding to lower Sr/Y ratios of 25.40-180.10.

5.2. Zircon U-Pb isotopic geochronology

5.2.1. Sample 12LN78-1 (Trondhjemitic gneiss, GPS position: N 42°12´00´´, E 124°36´04´´)

Zircon grains of this sample show stubby to elongated shapes, with lengths and length/width ratios of 80-150 μm and 1.2:1-2:1, respectively (Fig. 7A). On the cathodoluminescence (CL) images (Fig. 7A), most zircon grains display oscillatory or banded zoning (e.g., spots #03 and #17). Some grains display core-rim structures (e.g., spots #01 and #08), and the oscillatory zoned cores were eroded to irregular shapes and enveloped by prismatic and also oscillatory zoned rims. Twenty-four analyses were performed on twenty-four zircon grains, and all of them plot on concordia with apparent $^{207}Pb/^{206}Pb$ ages of 2612 ± 25 Ma to 2524 ± 31 Ma (Fig. 8A). These analyses show Th and U contents of 21-81 ppm and 71-127 ppm, respectively, yielding generally high Th/U ratios of 0.21-0.68. Six analyses on oscillatory zoned cores have $^{207}Pb/^{206}Pb$ ages of 2612 ± 25 Ma to 2582 ± 23 Ma, yielding a weighted mean age of 2592 ± 20 Ma (MSWD = 0.2). The remaining eighteen analyses from oscillatory zoned grains (without cores) or rims, show $^{207}Pb/^{206}Pb$ ages between 2574 ± 26 Ma and 2524 ± 31 Ma, which yield a weighted mean age of 2559 ± 11 Ma (MSWD = 0.27) and a concordia age of 2558 ± 4 Ma (MSWD = 0.00023) (Fig. 8A). Given that the trondhjemitic gneisses show intrusive relationships with regional supracrustal rocks (dated at ~2600-2570 Ma, Zhu et al., 2015 and our unpublished data; Fig. 3), the mean age of 2592 ± 20 Ma obtained from oscillatory zoned cores is taken as the age of xenocrystic zircons captured from the country rocks during magma ascent, whereas the age of 2558 ± 4 Ma from oscillatory zoned rims or grains is considered the crystallization age of magmatic precursor for the trondhjemitic gneiss. Similar crystallization ages of 2559-2553 Ma have been reported by Grant et al. (2009) for trondhjemitic gneisses in the northwest of Xiajiabao town.

5.2.2. Sample 13LB47-3 (Trondhjemitic gneiss, GPS position: N 42°06´38´´, E 124°24´08´´)

The stubby to elongated zircon grains in this sample have lengths and length/width ratios of 100-200 μm and 1.2:1-2.5:1, respectively (Fig. 7B). Their CL images (Fig. 7B) display core-rim structures, with bright structureless or oscillatory zoned cores surrounded by oscillatory zoned rims (e.g., spots #04 and #10). Some elongated and oscillatory zoned zircon grains don't have cores (e.g., spots #13 and #25). Twenty-five analyses were conducted on twenty-three zircon grains, and most plot on or close to concordia showing $^{207}Pb/^{206}Pb$ ages of 2712 ± 22 Ma to 2529 ± 20 Ma (Fig. 8B), though four analyses (i.e., spots #05, #09, #18, and #20) fall below the concordia (Fig. 8B). Th and U contents vary widely from 21 ppm to 1643 ppm and 37 ppm to 1868 ppm, respectively, corresponding to Th/U ratios mostly of 0.11-1.96, except for five younger analyses (spots #03, #06, #09, #13, and #23) with lower ratios of 0.02-0.08. These lower Th/U ratios and discordant features of some analyses may be the results of Pb-loss triggered by younger tectonothermal events.

Eight analyses on bright structureless or oscillatory zoned cores show apparent $^{207}Pb/^{206}Pb$ ages of 2712 ± 22 Ma to 2594 ± 20 Ma. Whereas two analyses (spots #10 and #12) give much older ages of 2712 ± 22 Ma and 2659 ± 24 Ma, the other six analyses for a coherent group with ages between 2625 ± 20 Ma and 2594 ± 20 Ma yield a weighted mean age of 2608 ± 16 Ma (MSWD = 0.28) and a concordia age of 2608 ± 5 Ma (MSWD = 0.002) (Fig. 8B). Similar to the trondhjemitic gneiss sample 12LN78-1, these older ages mostly on bright structureless (2712-2659 Ma) or oscillatory zoned cores (~2608 Ma) were considered to be those of zircon grains captured from the country rocks during magma ascent. A further seventeen analyses on oscillatory zoned zircons have $^{207}Pb/^{206}Pb$ ages of 2573 ± 21 Ma to

2529 ± 20 Ma, yielding an upper intercept age of 2559 ± 11 Ma (MSWD = 0.28) (Fig. 8B). Thirteen of these analyses are concordant and give a weighted mean age of 2558 ± 11 Ma (MSWD = 0.32) and a concordia age of 2558 ± 4 Ma (MSWD = 0.021), which are within error of the upper intercept age. Based on high Th/U ratios and oscillatory zoning, the age of 2558 ± 4 Ma is taken as the crystallization age for the magmatic precursor of the trondhjemitic gneiss.

5.2.3. Sample 13LB46-5 (Tonalitic gneiss, GPS position: N 42°13´23´´, E 124°37´57´´)

Zircon grains from this sample have oval to elongated shapes with lengths and length/width ratios of 80-150 μm and 1:1-2:1, respectively (Fig. 7C). CL images reveal that some zircon grains show core-rim structures with bright banded or oscillatory zoned cores enveloped by dark and structureless rims (e.g., spots #05 and #08). Other grains display dullish blurred zoning (e.g., spots #04 and #11) or dark structureless domains (e.g., spots #17 and #19) (Fig. 7C). Twenty-five analyses were conducted on twenty-five zircon grains. Most plot on or close to concordia, yielding apparent $^{207}Pb/^{206}Pb$ ages of 2646 ± 23 Ma to 2474 ± 21 Ma (Fig. 8C). Nine analyses fall below concordia, with one analysis showing an older apparent age of 2640 ± 22 Ma (spot #10) and the other eight analyses (spots #03, #06, #09, #12, #13, #17, #18, and #24) yielding ages between 2502 ± 22 Ma and 2481 ± 21 Ma (Fig. 8C). These analyses have variable Th and U contents from 14 ppm to 193 ppm and 68 ppm to 1803 ppm, respectively, yielding Th/U ratios mostly lower than 0.1 (0.02-0.09) but the six oldest analyses showing higher Th/U ratios of 0.20-1.39 (i.e., spots #05, #08, #10, #11, #15, and #16).

Based on internal structure and Th/U ratios, these analyses can be subdivided into three groups. The first age group is composed of three analyses (spots #08, #10, and #15) on bright

banded zoning cores, showing the oldest apparent $^{207}Pb/^{206}Pb$ ages of 2646 ± 23 Ma to 2592 ± 21 Ma (Figs. 7C and 8C). Their CL images are distinct from typical magmatic zircons crystallized from granitoid magmas with concentric or oscillatory zoning structures. Therefore, these apparently older ages are considered to be those of zircon grains captured from country rocks during magma ascent, which is consistent with their intrusive relationships with regional supracrustal metavolcanic rocks (~2600-2570 Ma; Zhu et al., 2015 and our unpublished data; Fig. 3). Four analyses on either oscillatory zoned (e.g., spot #05) or blurred zoned (e.g., spot #11) zircons constitute the second age group. They give apparent $^{207}Pb/^{206}Pb$ ages between 2543 ± 27 Ma and 2513 ± 21 Ma, yielding a weighted mean age of 2526 ± 22 Ma (MSWD = 0.33) and a concordia age of 2525 ± 6 Ma (MSWD = 0.0027). Considering their magmatic zircon-like internal structures and mostly high Th/U ratios (0.20-1.10, except for spot #04 with a lower value of 0.01), the concordia age of 2525 ± 6 Ma is taken to be the lower limit age for the magmatic precursor of the tonalitic gneiss. The third age group consists of eighteen analyses mostly on dullish blurred and zoned or dark structureless zircons (Fig. 7C). These analyses show $^{207}Pb/^{206}Pb$ ages ranging of 2512 ± 21 Ma to 2474 ± 21 Ma, and define a discordia with an upper intercept age of 2496 ± 6 Ma (MSWD = 1.06) (Fig. 8C). Ten concordant analyses yield a weighted mean age of 2498 ± 13 Ma (MSWD = 0.29), which may reflect the effects of regional high-grade metamorphism (Wu et al., 2013b; Peng et al., 2015).

5.2.4. Sample 13LB26-5 (Trondhjemitic gneiss, GPS position: N 41°47´48´´, E 124°49´04´´)

Zircon grains in this sample display oval to stubby shapes with lengths and length/width ratios of 50-120 μm and 1:1-1.2:1, respectively (Fig. 7D). CL images show dullish oscillatory

(or blurred) zoned or dark structureless structures, occasionally enveloped by bright rims (Fig. 7D). Twenty-five analyses were conducted on twenty-five zircons, and yield $^{207}Pb/^{206}Pb$ ages ranging from 2559 ± 22 Ma to 1765 ± 24 Ma (Fig. 8D). Th and U contents vary from 23 ppm to 330 ppm and 55 ppm to 2194 ppm, respectively, with Th/U ratios higher than 0.1 (0.12-0.74).

Two analyses on dark structureless domains (spots #03 and #09) yield the oldest $^{207}Pb/^{206}Pb$ ages of 2559 ± 22 Ma and 2553 ± 26 Ma (Figs. 7D and 8D). Their CL images are clearly distinct from magmatic zircons, which are therefore considered as xenocrystic zircons. The other twenty-three analyses define a discordia yielding an upper intercept age of 2505 ± 5 Ma (MSWD = 8.0) (Fig. 8D). Eleven analyses, plotting on or close to the upper intercept, give a weighted mean age of 2504 ± 14 Ma (MSWD = 0.29) and a concordia age of 2503 ± 4 Ma (MSWD = 0.021). Given mostly high Th/U ratios and oscillatory zonings of these analyses, the age of 2503 ± 4 Ma is considered to be close to the crystallization age of magmatic precursor to the trondhjemitic gneiss.

5.2.5. Sample 12LN59-1 (Monzogranitic gneiss, GPS position: N 42°12´25´´, E 124°54´25´´)

Zircon grains from this sample show stubby to elongated shapes, with lengths and length/width ratios of 100-250 μm and 1:1-2.5:1, respectively (Fig. 7E). They show core-rim structures on the CL images, with oscillatory zoned or structureless cores surrounded by structureless rims (e.g., spots #01 and #05). Twenty-eight analyses were conducted on twenty-two zircon grains, and all analyses plot on the concordia, with $^{207}Pb/^{206}Pb$ ages mostly of 2527 ± 55 Ma to 2490 ± 58 Ma (Fig. 8E). Th and U contents are of 88 ppm to 1261 ppm and 120 ppm to 3556 ppm, respectively, yielding generally high Th/U ratios of 0.12-1.65.

Three analyses on dark structureless cores (spots #05, #15 and #07) give older $^{207}Pb/^{206}Pb$ ages of 2778 ± 54 Ma to 2558 ± 54 Ma (Fig. 8E). Their CL images are clearly distinct from magmatic zircons, and are therefore considered as inherited or captured zircon grains. Seventeen analyses mostly on dark oscillatory zoned cores (e.g., spots #01 and #12) show similar $^{207}Pb/^{206}Pb$ ages of 2527 ± 54 Ma to 2502 ± 55 Ma (Fig. 7E). These analyses yield a weighted mean age of 2514 ± 26 Ma (MSWD = 0.022) and a concordia age of 2529 ± 3 Ma (MSWD = 1.8) (Fig. 8E). The concordia age is considered to be close to the crystallization age for the magmatic precursor to the monzogranitic gneiss (Fig. 8C). The other eight analyses on bright structureless rims or dark structureless cores (e.g., spots #11 and #23) have $^{207}Pb/^{206}Pb$ ages of 2499 ± 55 Ma to 2491 ± 54 Ma, yielding a weighted mean age of 2495 ± 38 Ma (MSWD=0.003). These data are interpreted to indicate the effects of the known regional metamorphic event at ~2495 Ma (Wu et al., 2013b; Peng et al., 2015).

5.2.6. Sample 12LN80-1 (Monzogranitic gneiss, GPS position: N 42°01´21´´, E 124°22´19´´)

Zircon grains from this sample generally display stubby to elongated shapes, with lengths and length/width ratios of 100-200 μm and 1:1-2:1, respectively (Fig. 7F). CL images of the zircons show dullish oscillatory zoning (e.g., spots #02 and #27), and some show core-rim structures, with the bright oscillatory zoned cores enveloped by dullish oscillatory zoned rims (e.g., spot #01). Thirty analyses were conducted on thirty zircons, and they all plot on concordia with $^{207}Pb/^{206}Pb$ ages of 2581 ± 25 Ma to 2491 ± 24 Ma (Fig. 8F). They have Th and U contents ranging from 14 ppm to 144 ppm and 47 ppm to 498 ppm, respectively, with Th/U ratios mostly of 0.10-0.46. Two analyses on bright oscillatory zoned cores (spots #01 and #04)

yield $^{207}Pb/^{206}Pb$ ages of 2581 ± 25 Ma and 2562 ± 23 Ma (Figs. 7F and 8F). Considering the high Th/U ratios (0.22-0.46) and bright oscillatory zoning inner structures, these ages are considered to be from inherited/captured zircons, which are nearly coeval with metavolcanic rocks (~2570 Ma) in the nearby Hongtoushan area (Fig. 2; Zhu et al., 2015). The other twenty-eight analyses mostly on dullish oscillatory zoned domains give $^{207}Pb/^{206}Pb$ ages of 2546 ± 27 Ma to 2491 ± 24 Ma, yielding a weighted mean age of 2515 ± 9 Ma (MSWD = 0.29) and a concordia age of 2515 ± 3 Ma (MSWD = 0.0001) (Figs. 7F and 8F). Given their mostly high Th/U ratios and magmatic zircon-like internal structures, the concordia age is considered to be close to the crystallization age of magmatic precursor to sample 12LN80-1.

5.3. Zircon Lu-Hf isotopes

The six dated samples (except for inherited or captured zircon grains), calculated at their respective apparent $^{207}Pb/^{206}Pb$ ages (t_1), show nearly consistent $^{176}Hf/^{177}Hf(t_1)$ values (0.281252 to 0.281339; 0.281294 to 0.281361; 0.281295 to 0.281345; 0.281333 to 0.281412; 0.281035 to 0.281140; and 0.281293 to 0.281369, respectively). One analysis (spot #09) of sample 12LN59-1 shows a lower $^{176}Hf/^{177}Hf(t_1)$ ratio of 0.280932. However, since down-hole isotopic variations during analyses can be reasonably precluded on the basis of generally small errors for the $^{176}Hf/^{177}Hf$ (0.000009-0.000010) and $^{176}Lu/^{177}Hf$ (0.000002-0.000013) ratios of analyses on sample 12LN59-1, these Lu-Hf isotopic data can be used for petrogenetic studies with confidence. If calculated to their crystallization ages (t_2), the six samples give $\varepsilon Hf(t_2)$ values and depleted mantle model ages ($T_{DM}(Hf)$) of +3.7 to +6.8 and 2602 Ma to 2719 Ma (12LN78-1, 2558 Ma); +5.2 to +7.6 and 2572 Ma to 2662 Ma (13LB47-3, 2558 Ma); +4.5 to

+6.2 and 2596 Ma to 2663 Ma (13LB46-5, 2525 Ma); +5.3 to +8.1 and 2505 Ma to 2611 Ma (13LB26-5, 2503 Ma); -4.7 to -1.0 and 2872 Ma to 3015 Ma (12LN59-1, 2529 Ma); and +4.2 to +6.9 and 2562 Ma to 2662 Ma (12LN80-1, 2515 Ma). Notably, most of these $\varepsilon Hf(t_2)$ values are close to the depleted mantle values, whereas sample 12LN59-1 shows remarkably enriched isotopic features (Fig. 9A). On the other hand, the three older analyses (#01, #07, and #12, t_2=2592 Ma) of sample 12LN78-1 yield $\varepsilon Hf(t_2)$ values of +5.0 to +7.2, with $T_{DM}(Hf)$ ages of 2616-2700 Ma. For sample 12LN59-1, the three older analyses (#05, #07, and #15) show $\varepsilon Hf(t_1)$ values of -2.6 to +0.1, with $T_{DM}(Hf)$ ages of 2855-3152 Ma. The near consistency of $T_{DM}(Hf)$ model ages for the three older zircon grains (2855-3152 Ma) and the magmatic zircon grains (2872-3015 Ma) for sample 12LN59-1 further precludes significant down-hole isotopic variations during analyses, indicating the involvement of some Mesoarchean continental materials in their petrogenesis. The two older grains (spots #01 and #04) for sample 12LN80-1 show $\varepsilon Hf(t_1)$ values of +6.9-+7.0 and $T_{DM}(Hf)$ modal ages of 2601-2615 Ma.

6. Discussion

6.1. Geochronologic framework of the Northern Liaoning Province

Zircon U-Pb age data reveal that the magmatic precursors of the tonalitic and trondhjemitic gneisses (DTT series) in the Qingyuan area formed during ~2558-2503 Ma, with generally three episodes at ~2558 Ma, ~2525 Ma, and ~2503 Ma, respectively (Figs. 3B-D and 8A-D). The magmatic precursors for the monzogranitic gneisses of the MM series were emplaced at ~2529-2515 Ma, which are statistically indistinguishable from the second episode of DTT series granitoid magmatism (Fig. 8E-F). The quartz dioritic gneisses and most of the

trondhjemitic-tonalitic gneisses show intense gneissosity, whereas the MM series samples and lesser volume of later tonalitic and trondhjemitic gneisses, are only weakly gneissic or massive (Fig. 3C-H). Thus, DTT series granitoid gneisses in the Qingyuan area formed dominantly at ~2558 Ma, whereas subordinate volumes of tonalitic and trondhjemitic gneisses as well as potassium-rich granitoid gneisses were generated at ~2529-2503 Ma.

Recent zircon U-Pb age data focusing on the Archean basement rocks of the NLP are listed in Supplementary Table 4, and the major magmatic events can be summarized as the following two volcanic-plutonic cycles (Fig. 10A): (1-a) eruption of voluminous volcanic rocks with basaltic to andesitic compositions at or prior to 2570 Ma; (1-b) quartz dioritic and TTG magmas (DTT series) emplaced during ~2559-2534 Ma; (2-a) a second episode of mafic volcanism developed locally in the Tangtu area at ~2530 Ma; and (2-b) a second episode of granitoid magmatism at ~2529-2496 Ma, forming dominantly quartz monzodioritic and monzogranitic rocks (MM series) and lesser volume of tonalitic and trondhjemitic gneisses.

Most basement rocks in the NLP were subjected to regional ~2510-2495 Ma high-grade metamorphism, indistinguishable in age from the second granitoid episode (Fig. 10B; Grant et al., 2009; Peng et al., 2015; Wu et al., 2016). Younger metamorphic ages of ~2479-2461 Ma, ~2427 Ma, and ~2350 Ma are also recorded by some basement rocks, which may be ascribed to the effects of multiple early Paleoproterozoic tectonothermal events along the northern margin of the EB (Fig. 10B; Liu et al., 2011; Wang et al., 2011, 2012b, 2013b, 2015a).

Minor zircon grains older than 2.7 Ga have also been recorded (~3100 Ma, ~2778 Ma, and ~2712 Ma) (Fig. 10C; this study and Zhu et al., 2015). Regionally, ~3.0-3.1 Ga lithological assemblages are well preserved in the adjoining Anshan-Benxi terrane, whereas ~2.7 Ga

rocks have been widely documented within the interior EB (Figs. 1B and 9B; Wan et al., 2013, 2014; Guo et al., 2015b). Older zircon grains with ages of 2674 ± 48 Ma to 2553 ± 26 Ma were also detected, possibly pointing to early volcanism as documented in EHP and WLP along the northern margin of the EB (Guo et al., 2013, 2015a; Wang et al., 2015a). Notably, preservation of minor xenocrystic zircons in TTG gneisses is common, especially when there is insufficient time for complete dissolution of the xenocrystic zircons that usually have higher melting temperature during magma ascent or emplacement (Wang et al., 2012b, 2013b; Meng et al., 2013; Bai et al., 2014a, 2015; Wu, 2014).

6.2. Petrogenesis of the late Neoarchean granitoid gneisses

6.2.1. Assessment of element mobility

Since the majority of late Neoarchean granitoid gneisses in the study area were subjected to amphibolite facies, and local granulite facies metamorphism (Figs. 2 and 4), assessment of element mobility is necessary prior to petrogenetic discussions (Polat and Hofmann, 2003; Wang et al., 2012a; Pearce, 2014). During sample collection, any outcrops with metasomatic or anatectic veins were avoided. In the chondrite-normalized REE and primitive mantle-normalized multi-element diagrams (Fig. 6), most samples of each group exhibit nearly parallel patterns of REEs (e.g., La, Sm, and Y) and high field strength elements (HFSEs, e.g., Nb, Ta, Ti, Zr, and Hf). The variable TREE contents and normalized REE patterns of the monzogranitic gneiss samples could be due to different source compositions or residual minerals (Fig. 6G). In contrast, the wide scatter of LILEs (especially of Ba and Rb) and Th probably reflects post-magmatic mobility, and these were not used in the petrogenetic

discussions (Wang et al., 2011, 2015a; Guo et al., 2013). Their mobility is also evidenced by trace elements versus Zr binary diagrams (Supplementary Fig. 1), in which linear correlations between La, Sm, Nb and Zr, contrast with the scatter of Ba, Rb, and Th contents (see Polat and Hofmann, 2003; Wang et al., 2011, 2015a). All the samples have loss on ignition (LOI) values of 0.29-2.98 wt.%, less than those of the altered samples (mostly >6 wt.%; Polat et al., 2002). These are consistent with the general absence of significant Ce anomalies ($Ce^*=Ce_N/Sqrt(La_N*Pr_N)$, mostly of 0.9-1.1), since rocks with Ce* values of 0.9-1.1 are considered as unaltered (Fig. 6; Polat and Hofmann, 2003).

6.2.2. The DTT series gneisses

The quartz dioritic gneiss samples are characterized by high Na_2O, Sr, and low K_2O, Y and Yb contents, with generally high Sr/Y and $(La/Yb)_N$ ratios, and plot in the field between adakitic rocks and classic arc-related basaltic-andesitic-dacitic-rhyolitic (BADR) volcanic suites (Fig. 11A and Supplementary Table 1). These share similar geochemical features with Phanerozoic adakites (Defant and Drummond, 1990; Martin et al., 2005). However, these adakitic signatures can be achieved by a variety of petrogenetic processes under diverse tectonic environments (Condie, 2005; Streck et al., 2007; Moyen, 2009; Wang et al., 2012b, 2013b). In the Mg# versus SiO_2 diagram (Fig. 11B), sample 12LN75-2 falls in the field of Phanerozoic adakites (Mg# value of 49.28), whereas sample 12LN58-1 plots in the field of experimentally-derived partial melts from metabasaltic rocks with a low value of 25.31 (Martin et al., 2005). Nonetheless, together with their low SiO_2 contents, these data indicate that simple intracrustal reworking cannot account for their petrogenesis, and mantle-derived

materials must have been involved. The MgO content of sample 12LN75-2 (3.37 wt.%) is also higher than those of crustal-derived melts (average MgO of 0.84 ± 0.44 wt.%; Zamora, 2000; Martin et al., 2005). No mafic magmas coeval with the quartz dioritic gneiss samples were detected in the Qingyuan area. Therefore, petrogenetic models involving magma mixing or fractional crystallization from a mafic magma are unlikely. The low TiO_2 contents (0.53-0.59 wt.%) of the samples are also inconsistent with their derivation from the partial melting of a slab melt-metasomatized mantle peridotite (Martin et al., 2010; Bai et al., 2014a). Accordingly, the quartz dioritic magmas were most likely generated by the partial melting of descending oceanic slabs, with the high MgO content and Mg# value stemming from the contamination of the adakitic magmas by the mantle wedge peridotites during their ascent. The low MgO content for sample 12LN58-1 may be ascribed to a lower degree of contamination by the mantle wedge peridotites or fractional crystallization. The enriched LREE patterns, moderately differentiated HREE patterns, and the lack of Eu and Sr anomalies, suggest that the oceanic slabs could have been metamorphosed to plagioclase-poor garnet amphibolites or eclogites prior to partial melting (Fig. 6A-B; Rollinson, 1993; Peng et al., 2015).

In comparison, nearly all the tonalitic and trondhjemitic gneiss samples fall into the field of experimentally-derived partial melts from metabasaltic rocks, indicating that mantle materials were not significantly involved in their parental magmas (Fig. 11B; Zamora, 2000; Martin et al., 2005; Wang et al., 2012b, 2013b). These samples show lower $(Yb)_N$ and dominantly higher $(La/Yb)_N$ values than the quartz dioritic gneiss samples, with generally positive Eu anomalies (Figs. 6C and 11A). On the basis of geochemical modelling, Bai et al. (2014a) proposed that the magmatic precursors for the late Neoarchean trondhjemitic

gneisses in the Eastern Hebei Province may be produced by hornblende fractionation from a dioritic magma. However, hornblende fractionation from a felsic magma system may result in decrease of TREE contents and Dy/Yb ratios with increasing SiO_2 contents (Rollinson, 1993). Compared to the quartz dioritic gneisses, the tonalitic and trondhjemitic gneisses show comparable or higher TREE contents and Dy/Yb ratios along with a roughly positive correlation between Dy/Yb and SiO_2, which argue against the fractional crystallization model (Fig. 11C). In the AFM (molar $Al_2O_3/(FeO_T+MgO)$) versus CFM (molar $CaO/(FeO_T+MgO)$) diagram (Fig. 11D), they fall largely in the field of partial melting products from metabasaltic to metatonalitic sources, with possible involvement of minor metagreywackes (Altherr et al., 2000). Partial melts generated from tonalitic rocks are mostly high-potassium granodioritic to monzogranitic in composition, precluding metatonalitic rocks as viable sources for the tonalitic and trondhjemitic gneiss samples (Moyen et al., 2003; Kumar et al., 2011). On the other hand, though the presence of minor ~2.7 Ga xenocrystic zircon grains, the four dated samples have highly positive $\varepsilon Hf(t_2)$ values (+3.7 to +8.1) close to the depleted mantle value (Figs. 7B and 9A). These data suggest that the tonalitic to trondhjemitic magmas may have been derived from the partial melting of dominantly late Neoarchean juvenile basaltic materials with minor greywackes. These samples have low to moderate Nb and Yb contents (mostly of 1.75-5.22 ppm and 0.12-1.13 ppm), analogous to the medium- to high-pressure TTG gneisses (Fig. 11E; Martin et al., 2005; Moyen, 2011). The high Al_2O_3 contents (mostly of 14.83-18.99 wt.%) and Gb/Yb ratios, as well as broadly positive Eu anomalies, all point to a high-pressure source region, with dominantly garnet, hornblende or clinopyroxene in the residues (Fig. 6C; Rollinson, 1993). Hornblende could be an important residue mineral, as evidenced by the low Nb/Ta

values (mostly of 5.98-16.83) (Fig. 11F; Foley et al., 2002). The positive Eu anomalies and high Sr concentrations and Sr/Y ratios suggest some plagioclase may be concentrated in the granitoid melts. Accordingly, the tonalitic and trondhjemitic gneisses could have been generated by the partial melting of dominantly juvenile basaltic materials (± minor greywackes) at pressure conditions where garnet was in equilibrium with the melt formed.

6.2.3. The MM series gneisses

Compared to the DTT series samples, the quartz monzodioritic gneiss samples display moderate $(La/Yb)_N$ ratios, higher Fe_2O_{3T} (5.80-11.80 vs. 2.06-8.21 wt.%), TiO_2 (0.54-1.28 vs. 0.20-0.59 wt.%), and P_2O_5 (0.22-0.57 vs. 0.03-0.18 wt.%) contents, which are common features of Archean sanukitoid series rocks (Fig. 12A; Martin et al., 2005; Heilimo et al., 2013). These data imply that a single crustal source cannot account for the genesis of these quartz monzodioritic gneisses, as ilmenite/rutile and apatite commonly preserved in the residual phases during partial melting of metabasalts would buffer Ti and P contents of the melts at lower values (Martin et al., 2005; Qian and Hermann, 2013). This is consistent with their mostly moderate to high MgO contents and Mg# values (except for samples P10YJD1, P10YJD2, P10YJD3, and P10YJD4), plotting above the experimentally-derived partial melts from metabasaltic rocks (Fig. 5D; Martin et al., 2005). Similar late Neoarchean Ti, P-rich plutonic rocks have been ascribed to mixing between underplated gabbroic magmas and crustal-derived melts (Yang et al., 2008; Nutman et al., 2011). Our geochemical modelling (Fig. 12B) reveals that samples 13LB33-3, 13LB39-1, 13LB42-5, and P10PLH2, P10PLH3, P10PLH4, P10PLH5 with high MgO contents show a linear correlation between La and La/V,

indicating a partial melting process (Schiano et al., 2010). The lack of correlations between Fe_2O_{3T}, TiO_2, and P_2O_5 with SiO_2 are also different from those of the 2490-2500 Ma gabbro-quartz monzonite-granite suites in Eastern Hebei with a magma mixing origin (Supplementary Table 1; Nutman et al., 2011). Considering their mildly depleted whole-rock εNd(t) values (+0.1-+0.5; Peng et al., 2015), we propose that the quartz monzodioritic magmas could have been produced by the partial melting of a mildly depleted mantle source. The lower $(Nb/La)_N$ and moderate $(Hf/Sm)_N$ ratios suggest the mantle source was metasomatized dominantly by slab-derived fluids prior to partial melting (Fig. 12C). The other four samples (P10YJD1, P10YJD2, P10YJD3, and P10YJD 4) with low MgO contents display a curved trend, following the trajectories of fractional crystallization or magma mixing (Fig. 12B). Nonetheless, the inverse correlation between CaO/Al_2O_3 and SiO_2, and near consistent Dy/Yb ratios with decreasing MgO contents, point to clinopyroxene (not hornblende) as the major fractionation phase from the quartz monzodioritic magmas (Fig. 12D-E; Rollinson, 1993). This observation is consistent with the increasing Zr/Sm ratios with decreasing MgO contents, which are likely effects of clinopyroxene fractionation (Supplementary Table 1; Rollinson, 1993). As revealed in Eastern Hebei, both igneous and metamorphic orthopyroxenes can be preserved in the charnockite series rocks under high grade metamorphism (Bai et al., 2015). Similarly, the presence of subhedral clinopyroxene crystals of inferred magmatic origin, in these metamorphosed quartz monzodioritic gneisses, is further support for the fractionation model (Fig. 4E). The low Eu_N/Eu^*_N values (0.58-0.73) of the low Mg quartz monzodioritic gneiss samples indicate some plagioclase fractionation.

The majority of monzogranitic gneiss samples display lower MgO and Mg# values, and

plot in the partial melting field of metabasaltic rocks (Fig. 5; Martin et al., 2005). Their Fe_2O_{3T}, TiO_2, and P_2O_5 contents are generally low (1.40-5.78 wt.%, 0.04-5.78 wt.%, and <0.14 wt.%, respectively), which are comparable with or lower than those of tonalitic to trondhjemitic gneisses of the DTT series (Supplementary Table 1). All the MM series samples have consistent Dy/Yb ratios, suggesting that the monzogranitic magmas were unlikely produced by hornblende fractionation from the quartz monzodioritic magma (Supplementary Table 1; Rollinson, 1993). All the above lines of evidence suggest insignificant involvement of mantle-derived magmas in the genesis of these monzogranitic gneiss samples. These samples show low CFM but high AFM values, suggesting their derivation from intracrustal recycling of dominantly metagreywackes (Fig. 12F; Rapp et al., 1999; Altherr et al., 2000; Wang et al., 2012b, 2013b). This is further confirmed by their moderate ($CaO+FeO_T+MgO+TiO_2$) contents (mostly of 2.10-6.06) and metaluminous to peraluminous features (A/CNK values of 0.99 to 1.76) (Douce, 1999). The two dated samples show contrasting zircon Lu-Hf isotopic compositions, i.e., highly positive $\varepsilon Hf(t_2)$ values of +4.2 to +6.9 for sample 12LN80-1, and negative values of -4.7 to -1.0 for sample 12LN59-1. These data indicate that monzogranitic gneiss samples from north of the town of Nanzamu are dominantly sourced from juvenile crustal materials, whereas recycling of ancient crustal materials was locally involved in the magmatic genesis of samples in the north of Qingyuan county (Figs. 2 and 9). Moreover, samples north of Qingyuan county are characterized by higher Yb and Y contents and consistently negative Eu and Sr anomalies (Fig. 6G-H), compared to Nanzamu samples. Therefore, plagioclase crystals could be important residue minerals in the source region, implying a middle crustal source (Liu et al., 2004; Bai et al.,

2015). The concave-upward chondrite-normalized REE patterns with mostly low Yb and Y contents and positive Eu anomalies for the Nanzamu samples are compatible with a garnet and hornblende-bearing residue lithology at middle to lower crustal levels (Fig. 6G-H; Rollinson, 1993; Wang et al., 2012b, 2013b). The moderate K_2O/Na_2O ratios (mostly of 0.84-1.56) and high Na_2O contents (mostly >3.57 wt.%) suggest that the parental magmas for these monzograntic gneiss samples could have stemmed from hydrous melting of metagreywackes, with preferential decomposition of plagioclase over mica in the source region (Sawyer et al., 2011; Huang et al., 2015). The presence of some euhedral xenocrystic zircon grains also implies a low-temperature felsic melt (Figs. 7E-F and 8E-F). Accordingly, these monzogranitic gneiss samples were produced by hydrous partial melting of metagreywackes with different crustal resident ages at middle to lower crustal levels.

6.3. Late Neoarchean geodynamic processes of the Northern Liaoning Province

The oldest exposed units in the NLP are metamorphosed tholeiitic to calc-alkaline basaltic to andesitic rocks erupted at or prior to 2570 Ma (Figs. 10A and 13A-B; Wan et al., 2005a,b; Wang et al., 2015a,e). Petrogenetic studies reveal that these metavolcanic rocks can be subdivided into three subgroups (Fig. 13C-D): (a) MORB-type metabasaltic rocks (high $(Nb/La)_{PM}$ (0.90-1.18) and low $(La/Sm)_N$ (1.33-1.53)) derived from partial melting of mildly depleted mantle sources unaffected by subduction-derived materials; (B) island arc tholeiite (IAT)-type metabasaltic rock with lower $(Nb/La)_{PM}$ (0.83) and higher $(La/Sm)_N$ (1.90) ratios than the MORB samples, likely generated by partial melting of an enriched mantle source metasomatized by minor subduction-derived fluids or melts; and (C) metamorphosed

calc-alkaline basaltic (CAB) to andesitic rocks showing the lowest $(Nb/La)_{PM}$ (0.08-0.55) and highest $(La/Sm)_N$ (2.47-5.30) ratios, probably sourced from an enriched mantle source strongly metasomatized by subduction-derived fluids or melts. Accordingly, adiabatic upwelling of asthenospheric mantle beneath an Archean spreading ridge (≥2570 Ma) gave rise to the N-MORB-like rocks and juvenile oceanic lithospheric mantle (Fig. 14A). Subsequently during the intra-oceanic subduction stage, the oceanic lithospheric mantle was gradually metasomatized by slab-derived fluids, generating other tholeiitic to calc-alkaline basaltic to andesitic rocks (Fig. 14B; Polat, 2013; Wang et al., 2015a).

The above metavolcanic rocks and the dominantly juvenile features of late Neoarchean plutonic granitoid gneisses in the NLP (except for sample 12LN59-1) (Fig. 9), suggest that they should constitute the northeastern segment of the ~2.64-2.52 Ga intra-oceanic arc system along the northwestern margin of the EB (Wang et al., 2015a). With gradual maturation of this arc system, partial melting of descending slabs at ~2550-2530 Ma led to the generation of the quartz dioritic rocks (Fig. 14C). Upwelling mantle further triggered partial melting of lower arc crustal materials, generating the tonalitic and trondhjemitic rocks.

Monzogranitic gneiss samples show contrasting zircon $\varepsilon Hf(t_2)$ values, reflecting derivation from partial melting of dominantly metagreywackes with different crustal resident ages (Figs. 9 and 12F). Minor xenocrystic zircon grains (≥ 2.7 Ga) detected to the north of the Hunhe Fault (Fig. 10C) further suggest that the genesis of these monzogranitic gneisses involved both reworking of juvenile and ancient continental crust materials. Considering that this late episode of magmatism was roughly coeval with regionally ~2510-2495 Ma high grade metamorphism (Fig. 10), we propose that these tectonothermal events may be related to the accretion of the

proposed intra-oceanic arc system onto the ancient continental margin of the Anshan-Benxi-Southern Jilin Province (SJP) terrane to the south and east (Fig. 14D; Zhang et al., 2013a; Wang et al., 2015a; Guo et al., 2015b). The partially overriding of the arc system to the continental margin and the induced slab rollback processes triggered upwelling of the hot asthenospheric mantle. This upwelling caused partial melting of the metasomatized lithospheric mantle, as well as both juvenile arc crust and ancient continental margin materials, leading to the generation of the quartz monzodioritic and monzogranitic rocks in the study area (Nutman et al., 2015). Notably, minor trondhjemitic gneisses formed during the dominant episode of potassium-rich granitoid magmatism (Fig. 10A), and the magmatic precursors of these trondhjemitic gneisses might be derived from either partial melting of metagreywackes and volcanic rocks or partial melting of Na-rich metamorphic sedimentary rocks that have more muscovite (Guo et al., 2015b). On the other hand, the nearly coherent chronological frameworks and isotopic compositions of the mostly amphibolite and locally granulite facies metamorphosed regions (e.g., Xianjinchang area) in the NLP implies that they may represent different crustal levels of a single arc system (Figs. 9-10), similar to those in the adjacent Western Liaoning Province (Wang et al., 2015a).

Accordingly, the NLP experienced a complex late Neoarchean subduction-related crustal evolution history, i.e., from mid-ocean ridge spreading, through initiation and gradual maturation of the intra-oceanic arc system, to the final arc-continent accretion, equivalent to the late Neoarchean intra-oceanic arc system along the northwestern EB (Figs. 1B and 14).

6.4. Implications of ~2.6-2.5 Ga subduction-related crustal growth in the Eastern Block

As stated above, the NLP records a major episode of crustal growth during late Neoarchean, through the generation of a major intra-oceanic arc system along the northwestern EB (Fig. 1B; Wang et al., 2015a). ~2.6-2.5 Ga metabasaltic rocks and dioritic gneisses within the interior EB (e.g., Fuping and Hengshan complexes, Western Shandong, and Jiaodong terrane), may also record intense late Neoarchean crustal growth (Wang et al., 2009; Wan et al., 2010; Meng et al., 2013; Peng et al., 2013; Shan et al., 2015). In the adjacent Yinshan Block (Fig. 1A), ~2.54-2.49 Ga supracrustal metabasaltic rocks (with possible komatiites) and plutonic granitoid gneisses have been inferred to record late Neoarchean subduction-related crustal growth (Ma et al., 2013, 2014). These events may extend to the Tarim craton based on the inferred affinities with the NCC (Long et al., 2010; Ge et al., 2013, 2014; Zhang et al., 2013b). Late Neoarchean lateral continental accretion and crustal growth has also been well documented in southern India, where the southern margin of Dharwar craton witnessed vigrous arc-arc and arc-continent collision processes, as evidenced by intra-oceanic arcs, dismembered ophiolites, and microcontinents (Santosh et al., 2013; Anand et al., 2014; Samual et al., 2014; Yang et al., 2015). In the Vestfold Hills terrane of east Antarctica, ~2520-2450 Ma gabbroic to granitoid rocks along with granulite-facies metamorphism and ~2.7-2.6 Ga detrital zircon age populations, suggest this terrane may be the missing link of NCC with a major episode of crustal growth during the late Neoarchean (Zhao et al., 2003, 2012; Clark et al., 2012). With respect to southern Australia, ~2555-2410 Ma magmatism, sedimentation, and metamorphism were identified in the Gawler Craton, likely evolved under a continental arc setting (Cawood and Korsch, 2008; Reid et al., 2014a, b). Similar ~2.5 Ga tectonothermal events and crustal growth may be also preserved in North

Australia, Terra Adelie Craon in Antarctica, and Sask craton in Canada (Reid et al., 2014a).

Thus, the late Neoarchean period was likely marked by widespread convergent plate margin magmatism and crustal growth, leading to accretionary margin and ultimately collisional orogenesis resulting in the assembly of these cratonic fragments (Bleeker, 2003; Zhao et al., 2003; Piper, 2010; Strand and Köykkä, 2012; Pehrsson et al., 2013).

7. **Conclusions**

(1) Late Neoarchean granitoid gneisses in the Northern Liaoning Province can be subdivided into two major episodes, i.e., ~2559-2534 Ma strongly gneissic quartz dioritic and tonalitic to trondhjemitic gneisses (DTT series); and ~2529-2495 Ma weakly gneissic to massive quartz monzodioritic and monzogranitic gneisses (MM series), with subordinate tonalitic to trondhjemitic gneisses. Most of the basement units were subjected to ~2510-2495 Ma high-grade metamorphism.

(2) Most granitoid gneisses in the Northern Liaoning Province show highly depleted zircon $\varepsilon Hf(t_2)$ values, suggesting a major late Neoarchean episode of crustal growth. Whereas some monzogranitic gneisses have negative zircon $\varepsilon Hf(t_2)$ values, together with the occurrence of ~3.1-2.7 Ga xenocrystic or inherited zircon grains, indicating that minor ancient continental materials sourced from the Anshan-Benxi terrane may have been involved.

(3) The quartz dioritic and tonalitic to trondhjemitic gneiss samples were produced by the partial melting of either oceanic slabs metamorphosed to plagioclase-poor garnet amphibolites or eclogites or juvenile metabasaltic rocks of lower arc crust. In comparison, the quartz monzodioritic gneiss samples were generated by the partial melting of a depleted mantle

source metasomatized chiefly by slab-derived fluids, with some samples showing clinopyroxene and plagioclase fractionation. The monzogranitic gneiss samples were produced by the partial melting of metagreywackes with different crustal resident ages at middle to lower crustal levels.

(4) The Northern Liaoning Province experienced late Neoarchean subduction-related crust-mantle interactions. Arc-continent accretion and possibly slab rollback processes may have triggered reworking of both juvenile arc crust and minor ancient continental margin materials along the northern margin of Eastern Block.

Acknowledgments

Constructive suggestions and comments by M. Santosh and one anonymous reviewer, and by editor Guochun Zhao led to significant improvements in the quality of the manuscript. We also appreciate Dr. L. Su for assistance with zircon U-Pb isotopic and trace element analyses at the Geological Lab Center, China University of Geosciences, Beijing, Dr. Z.C. Hu for assistance with zircon Lu-Hf isotopic analyses at the state Key Laboratory of Geological Processes and Mineral Resources, China University of Geosciences in Wuhan, and B. Yang, L.B. Gu and M. Liu for help with whole-rock major and trace element analyses at the Key Laboratory of Orogenic Belts and Crustal Evolution, Peking University and the Research Institute of Uranium Geology, Beijing, respectively. This study is financially supported by the National Natural Science Foundation of China (Grant Nos. 41272209, 41472165, 41502179, 41530207) and the Central University Basic Scientific Research Business Expenses of China University of Geosciences (Beijing) (Grant No. 2652015038).

References

Altherr, R., Holl, A., Hegner, E., 2000. High-potassium, calc-alkaline I-type plutonism in the European Variscides: Northern Vosges (France) and northern Schwarzwald (Germany). Lithos 50, 51-73.

Anand, R., Balakrishnan, S., Kooijman, E., Mezger, K., 2014. Neoarchean crustal growthby accretionary processes: evidence from combined zircon-titanite U-Pb isotope studies on granitoid rocks around the Hutti greenstone belt, eastern Dharwar Craton, India. Journal of Asian Earth Sciences 79, 72-85.

Anderson, T., 2002. Correlation of common lead in U-Pb analyses that do not report 204Pb. Chemical Geology 192, 59-79.

Bai, X., Liu, S.W., Guo, R.R., Zhang, L.F., Wang, W., 2014a. Zircon U-Pb-Hf isotopes and geochemistry of Neoarchean dioritic–trondhjemitic gneisses, Eastern Hebei, North China Craton: Constraints on petrogenesis and tectonic implications. Precambrian Research 251, 1-20.

Bai, X., Liu, S.W., Zhang, L.F., Yan, M., Wang, W., Guo, R.R., Guo, B.R., 2014b. Geological event series of Early Precambrian complex in South Fushun area, Liaoning Province. Acta Petrologica Sinica 30, 2905-2924 (in Chinese with English abstract).

Bai, X., Liu, S.W., Guo, R.R., Wang, W., 2015. Zircon U-Pb-Hf isotopes and geochemistry of two contrasting Neoarchean charnockitic rock series in Eastern Hebei, North China Craton: Implications for petrogenesis and tectonic setting. Precambrian Research 267, 72-93.

Bai, X., Liu, S.W., Guo, R.R., Wang, W., 2016. A Neoarchean arc-back-arc system in Eastern

Hebei, North China Craton: constraints from zircon U-Pb-Hf isotopes and geochemistry of dioritic-tonalitic-trondhjemitic-granodioritic (DTTG) gneisses and felsic paragneisses. Precambrian Research 273, 90-111.

Barker, F., 1979. Trondhjemite: definition, environment and hypotheses of origin. In: Barker, F. (Ed.), Trondhjemites, Dacites, and Related Rocks. Elsevier, Amsterdam, pp. 1-12.

Belousova, E.A., Kostitsyn, Y.A., Griffin, W.L., Begg, G.C., O'Reilly, S.Y., Pearson, N.J., 2010. The growth of the continental crust: constraints from zircon Hf-isotope data. Lithos 119, 457-466.

Bleek, W., 2003. The late Archean record: a puzzle in ca. 35 pieces. Lithos 71, 99-134.

Blichert-Toft, J., Albarède, F., 1997. The Lu-Hf geochemistry of chondrites and the evolution of the mantle-crust system. Earth and Planetary Science Letters 148, 243-258.

Cawood, P.A., Kröner, A. and Pisarevsky, S.A., 2006. Precambrian Plate Tectonics: Criteria and Evidence. GSA Today 16, 4-11.

Cawood, P.A., Korsch, 2008. Assembling Australia: Proterozoic building of a continent. Precambrian Research 166, 1-35.

Cawood, P.A., Hawkesworth, C.J., Dhuime, B., 2013. The continental record and the generation of continental crust. Geological Society of American Bulletin 125, 14-32.

Clark, C., Kinny, P.D., Harley, S.L., 2012. Sedimentary provenance and age of metamorphism of the Vestford Hills, East Antarctica: Evidence for a piece of Chinese Antarctica? Precambrian Research 196-197, 23-45.

Condie, K.C., 1998. Episodic continental growth and supercontinents: a mantle avalanche connection? Earth and Planetary Science Letters 163, 97-108.

Condie, K.C., 2005. TTGs and adakites: are they both slab melts? Lithos 80, 33-44.

Condie, K.C., O'Neil, C., 2010. The Archean-Proterozoic boundary: 500 My of tectonic transition in earth history. American Journal of Science 310, 775-790.

Condie, K.C., Kröner, A., 2013. The building blocks of continental crust: Evidence for a major change in the tectonic setting of continental growth at the end of the Archean. Gondwana Research 23, 394-402.

Cui, P.L., Sun, J.F., Sha, D.M., 2013. Oldest zircon xenocryst (4.17 Ga) from the North China Craton. International Geology Reviews 55, 1902-1908.

Defant, M.J., Drummond, M.S., 1990. Derivation of some modern arc magmas by melting of young subducted lithosphere. Nature 347, 662-665.

Dhuime, B., Hawkesworth, C., Cawood, P., 2011. When continents formed. Science 331, 154-155.

Dhuime, B., Hawkesworth, C.J., Cawood, P.A., Storey, C.D., 2012. A change in the geodynamic of continental growth 3 billion years ago. Science 335, 1334-1336.

Dhuime, B., Wuestefeld, A., Hawkesworth, C.J., 2015. Emergence of modern continental crust about 3 billion years ago. Nature Geoscience 8, 552-555.

Douce, A.E.P., 1999. What do experiments tell us about the relative contributions of crust and mantle to the origin of granitic magmas? Geological Society, London, Special Publications 168, 55-75.

Foley, S., Tiepolo, M., Riccardo, V., 2002. Growth of early continental crust controlled by melting of amphibolite in subduction zones. Nature 417, 837-840.

Ge, R.F., Zhu, W.B., Wu, H.L., He, J.W., Zheng, B.H., 2013. Zircon U-Pb ages and Lu-Hf

isotopes of Paleoproterozoic metasedimentary rocks in the Korla Complex, NW China: implications for metamorphic zircon formation and geological evolution of the Tarim Craton. Precambrian Research 231, 1-18.

Ge, R.F., Zhu, W.B., Wilde, S.A., Wu, H.L., He, J.W., Zheng, B.H., 2014. Archean magmatism and crustal evolution in the northern Tarim Craton: insights from zircon U-Pb-Hf-O isotopes and geochemistry of ~2.7 Ga orthogneisses and amphibolite in the Korla Complex. Precambrian Research 252, 145-165.

Geng, Y.S., Liu, F.L., Yang, C.H., 2006. Magmatic event at the end of the Archean in eastern Hebei Province and its geological implication. Acta Geologica Sinica-English Edition 80, 819-833.

Geng, Y.S., Shen, Q.H., Ren, L.D., 2010. Late Neoarchean to early Paleoproterozoic magmatic events and tectonothermal systems in the North China Craton. Acta Petrologica Sinica 26, 1945-1966 (in Chinese with English abstract).

Geng, Y.S., Du, L.L., Ren, L.D., 2012. Growth and reworking of the early Precambrian continental crust in the North China Craton: Constraints from zircon Hf isotopes. Gondwana Research 21, 517-529.

Grant, M.L., Wilde, S.A., Wu, F.Y., Yang, J.H., 2009. The application of zircon cathodoluminescence imaging, Th-U-Pb chemistry and U-Pb ages in interpreting discrete magmatic and high-grade metamorphic events in the North China Craton at the Archean/Proterozoic boundary. Chemical Geology 261, 155-171.

Griffin, W.L., Pearson, N.J., Belousova, E., Jackson, S.E., van Achterbergh, E., O'Reilly, S.Y., Shee, S.R., 2000. The Hf isotope composition of cratonic mantle: LAM-MC-ICPMS

analysis of zircon megacrysts in kimberlites. Geochimica et Cosmochimica Acta 64, 133-147.

Griffin, W.L., Belousova, E.A., O'Neill, C., O'Reilly, S.Y., Malkovets, V., Pearson, N.J., Spetsius, S., Wilde, S.A., 2014. The world turns over: Hadean-Archean crust-mantle evolution. Lithos 189, 2-15.

Guo, J.H, O'Brien, P.J., Zhai, M.G., 2002. High-pressure granulites in the Sanggan area, North China craton: metamorphic evolution, P-T paths and geotectonic significance. Journal of Metamorphic Geology 20, 741-756.

Guo, J.H., Sun, M., Chen, F.K., Zhai, M.G., 2005. Sm-Nd and SHRIMP U-Pb zircon geochronology of high-pressure granulites in the Sanggan area, North China Craton: timing of Paleoproterozoic continental collision. Journal of Asian Earth Sciences 24, 629-642.

Guo, J.H., Peng, P., Chen, Y., Jiao, S.J., Windley, B.F, 2012. UHT sapphirine granulite metamorphism at 1.93-1.92 Ga caused by gabbronorite intrusions: Implications for tectonic evolution of the northern margin of the North China Craton. Precambrian Research 222, 124-142.

Guo, R.R., Liu, S.W., Santosh, M., Li, Q.G., Bai, X., Wang, W., 2013. Zircon U-Pb-Hf isotopes and geochemistry of Neoarchean dioritic-trondhjemitic gneisses, Eastern Hebei, North China Craton: Constraints on petrogenesis and tectonic implications. Gondwana Research 24, 664-686.

Guo, R.R., Liu, S.W., Wyman, D., Bai, X., Wang, W., Yan, M., Li, Q.G., 2015a. Neoarchean subduction: A case study of arc volcanic rocks in Qinglong-Zhuzhangzi area of the

Eastern Hebei Province, North China Craton. Precambrian Research 264, 36-62.

Guo, B.R., Liu, S.W., Zhang, J., Yan, M., 2015b. Zircon U-Pb-Hf isotope systematics and geochemistry of Helong granite-greenstone beltin Southern Jilin Province, China: Implications for Neoarchean crustal evolution of the northeastern margin of North China Craton. Precambrian Research 271, 254-277.

Hawkerworth, C., Cawood, P., Kemp, T., Storey, C., Dhuime, B., 2009. A matter of preservation. Science 323, 49-50.

Hawkesworth, C.J., Dhuime, B., Pietranik, A.B., Cawood, P.A., Kemp, A.I.S., Storey, C.D., 2010. The generation and evolution of the continental crust. Journal of the Geological Society, London 167, 229-248.

Heilimo, E., Jaana, H., Andersen, T., Huhma, H., 2013. Neoarchean crustal recycling and mantle metasomatism: Hf-Nd-Pb-O isotope evidence from sanukitoids of the Fennoscandian shield. Precambrian Research 228, 250-266.

Herzberg, C., Condie, K.C., Korenaga, J., 2010. Thermal history of the Earth and its petrological expression. Earth and Planetary Science Letters 292, 79-88.

Hu, Z.C., Liu, Y.S., Gao, S., Liu, W.G., Zhang, W., Tong, X.R., Lin, L., Zong, K.Q., Li, M., Chen, H.H., Zhou, L., Yang, L., 2012. Improved in situ Hf isotope ratio analysis of zircon using newly designed X skimmer cone and jet sample cone in combination with the addition of nitrogen by laser ablation multiple collector ICP-MS. Journal of Analytical Atomic Spectrometry 27, 1391-1399.

Huang, H.Q., Li, X.H., Li, Z.X., Li, W.X., 2015. Formation of the Jurassic South China Large Granitic Province: insights from the genesis of the Jiufeng pluton. Chemical Geology 401,

43-58.

Johnson, T.E., Brown, M., Kaus, B.J.P., VanTongeren, J.A., 2013. Delamination and recycling of Archaean crust caused by gravitational instabilities. Nature Geoscience 7, 47-52.

Kawai, K., Tsuchiya, T., Tsuchiya, J., Maruyama, S., 2009. Lost primordial continents. Gondwana Research 16, 581-586.

Kumar, K.V., Ernst, W.G., Leelanandam, C., Wooden, J.L., Grove, M.J., 2011. Origin of ~2.5 Ga potassic granite from the Nellore Schist Belt, SE India: textural, cathodoluminescence, and SHRIMP U-Pb data. Contributions to Mineralogy and Petrology 162, 867-888.

LaFlèche, M.R., Camire, G., Jenner, G.A., 1998. Geochemistry of post-Acadian, Carboniferous continental intraplate basalts from the Maritimes basin, Magdalen islands, Quebec, Canada. Chemical Geology 148, 115-136.

Li, J.J., Shen, B.F., 2000. Geochronology of Precambrian continent crust in Liaoning Province and Jilin Province. Progress in Precambrian Research 23, 244-249 (in Chinese with English abstract).

Li, S.Z., Zhao, G.C., 2007. SHRIMP U-Pb zircon geochronology of the Liaoji granitoids: constraints on the evolution of the paleoproterozoic Jiao-Liao-Ji belt in the eastern block of the North China Craton. Precambrian Research 158, 1-16.

Li, S.S., Santosh, M., Cen, K., Teng, X.M., He, X.F., 2015. Neoarchean convergent margin tectonics associated with microblock amalgamation in the North China Craton: Evidence from The Yishui Complex. Gondwana Research, doi: 10.1016/j.gr.2015.11.004.

Liu, D.Y., Nutman, A.P., Compston, W., Wu, J.S., Shen, Q.H., 1992. Remmants of ≥3800 Ma

crust in the Chinese part of the Sino-Korean Craton. Geology 20, 339-342.

Liu, S.W., Pan, Y.M., Li, J.H., Zhang, J., Li, Q.G., 2002. Geological and isotopic geochemical constraints on the evolution of the Fuping Complex, North China Craton. Precambrian Research 117, 41-56.

Liu, S.W., Pan, Y.M., Xie, Q.L., Zhang, J., Li, Q.G., 2004. Archean geodynamics in the Central Zone, North China craton: constraints from geochemistry of two contrasting series of granitoids in the Fuping and Wutaishan complexes. Precambrian Research 130, 229-249.

Liu, S.W., Pan, Y.M., Xie, Q.L., Zhang, J., Li, Q.G., 2005. Geochemistry of the Paleoproterozoic Nanying granitic gneisses in the Fuping complex: implications for the tectonic evolution of the Central zone, North China Craton. Journal of Asian Earth Sciences 24, 643-658.

Liu, S.W., Zhao, G.C., Wilde, S.A., Shu, G.M., Sun, M., Li, Q.G., Tian, W., Zhang, J., 2006. Th-U-Pb monazite geochronology of the Lvliang and Wutai complexes: constraints on the tectonothermal evolution of the Trans-North China Orogen. Precambrian Research 148, 205-225.

Liu, D.Y., Wilde, S.A., Wan, Y.S., Wu, J.S., Zhou, H.Y., Dong, C.Y., Yin, X.Y., 2008. New U-Pb and Hf isotopic data confirm Anshan as the oldest preserved segment of the North China Craton. American Journal of Science 308, 200-231.

Liu, S.W., Santosh, M., Wang, W., Bai, X., Yang, P.T., 2011. Zircon U-Pb chronology of the Jianping Complex: Implications for the Precambrian crustal evolution history of the northern margin of North China Craton. Gondwana Research 20, 48-63.

Liu, S.W., Zhang, J., Li, Q.G., Zhang, L.F., Wang, W., Yang, P.T., 2012. Geochemistry and U-Pb zircon ages of metamorphic volcanic rocks of the Paleoproterozoic Lüliang Complex and constraints on the evolution of the Trans-North China Orogen, North China Craton. Precambrian research 222-223, 173-190.

Liu, J.H., Liu, F.L., Ding, Z.J., Liu, C.H., Yang, H., Liu, P.H., Wang, F., Meng, E., 2013. The growth, reworking and metamorphism of early Precambrian crust in the Jiaobei terrane, the North China Craton: constraints from U-Th-Pb and Lu-Hf isotopic systematics, and REE concentrations of zircon from Archean granitoid gneisses. Precambrian Research 224, 287-303.

Liu, C.H., Zhao, G.C., Liu, F.L., et al., 2014. Zircon U-Pb and Lu-Hf isotopic and whole-rock geochemical constraints on the provenance and age of the Shuangshanzi and Qinglonghe Groups in Eastern Hebei: Implications for the tectonic evolution of the Eastern Block. Precambrian Research 255, 699-715.

Long, X.P., Yuan, C., Sun, M., Zhao, G.C., Xiao, W.J, Wang, Y.J., Yang, Y.H., Hu, A.Q., 2010. Archean crustal evolution of the northern Tarim Craton, NW China: zircon U-Pb and Hf isotopic constraints. Precambrian Research 180, 272-284.

Ludwig, K.R., 2003. Berkeley Geochronology Center Special Publication, vol. 4.

Luo, Y., Sun, M., Zhao, G.C., Li, S.Z., Xu, P., Ye, K., Xia, X.P., 2004. LA-ICP-MS U-Pb zircon ages of the Liaohe Group in the Eastern Block of the North China Craton: constraints on the evolution of the Jiao-Liao-Ji Belt. Precambrian Research 134, 349-371.

Ma, X.D., Guo, J.H., Liu, F., Qian, Q., Fan, H.R., 2013. Zircon U-Pb ages, trace elements and Nd-Hf isotopic geochemistry of Guyang sanukitoids and related rocks: Implications for

the Archean crustal evolution of the Yinshan Block, North China Craton. Precambrian Research 230, 61-78.

Ma, X.D., Fan, H.R., Santosh, M., Guo, J.H., 2014. Chronology and geochemistry of Neoarchean BIF-type iron deposits in the Yinshan Block, North China Craton: Implications for oceanic ridge subductionOre Geology Reviews 63, 405-417.

Maniar, P.D., Piccoli, P.M., 1989. Tectonic discrimination of granitoids. Geological Society of American Bulletin 101, 635-643.

Martin, H., 1986. Effect of steeper Archean geothermal gradient on geochemistry of subduction-zone magmas. Geology 14, 753-756.

Martin, H., Smithies, R.H., Moyen, J. F., Champion, D., 2005. An overview of adakite, tonalite-trondhjemite-granodiorite (TTG), and sanukitoid: relationships and some implications for crust evolution. Lithos 79, 1-24.

Martin, H., Moyen, J.F., Rapp, R., 2010. The sanukitoid series: magmatism at the Archaean–Proterozoic transition. Sixth Hutton Symposium on the Origin of Granites and Related Rocks: Proceedings of a Symposium Held in Stellenbosch, South Africa, 2–6 July 2007. Cambridge University Press, p. 15.

Meng, E., Liu, F.L., Liu, J.H., Liu, P.H., Cui, Y., Liu, C.H., Yang, H., Wang, F., Shi, J.R., Kong, Q.B., Lian, T., 2013. Zircon U-Pb and Lu-Hf isotopic constraints on Archean crustal evolution in the Liaonan complex of northeast China. Lithos 177, 164-183.

Mints, M.V., Dokukina, K.A., Konikov, A.N., 2014. The Meso-Neoarchaean Belomorian eclogite province: Tectonic position and geodynamic evolution. Gondwana Research 25, 561-584.

Moyen, J.F., Martin, H., Jayananda, M., Auvray, B., 2003. Late Archaean granites: a typology based on the Dharwar Craton (India). Precambrian Research 127, 103-123.

Moyen, J.F., 2009. High Sr/Y and La/Yb ratios, the meaning of the "adakitic signature". Lithos 112, 556-574.

Moyen, J.F., 2011. The composite Archaean grey gneisses: petrological significance, and evidence for a non-unique tectonic setting for Archaean crustal growth. Lithos 123, 21-36.

Nutman, A.P., Wan, Y.S., Du, L.L., Friend, C.R.L., Dong, C.Y., Xie, H.Q., Wang, W., Sun, H.Y., Liu, D.Y., 2011. Multistage late Neoarchaean crustal evolution of the North China Craton, eastern Hebei. Precambrian Research 189, 43-65.

Nutman, A.P., Bennett, V.C., Friend, C.R.L., Yi, K., Lee, S.R., 2015. Mesoarchaean collision of Kapisilik terrane 3070 Ma juvenile arc rocks and >3600 Ma Isukasia terrane continental crust (Greenland). Precambrian Research 258, 146-160.

O'Connor, J.T., 1965. A classification for quartz-rich igneous rocks based on feldspar ratios. U.S. Geological Survey Professionnal Paper, 525, pp. 79-84.

O'Neill, C., Lenardic, A., Moresi, L., Torsvik, T.H., and Lee, C.T.A., 2007. Episodic Precambrian subduction: Earth and Planetary Science Letters 262, 552-562.

Pearce, J.A., Harris, N.B.W., Tindle, A.G., 1984. Trace element discrimination diagrams for the tectonic interpretation of granitic rocks. Journal of Petrology 25, 956-983.

Pearce, J.A., 2014. Geochemical Fingerprinting of the Earth's Oldest Rocks. Geology 42, 175-176.

Pehrsson, S.J., Berman, R.G., Eglington, B., Rainbird, R., 2013. Two Neoarchean

supercontinents revisited: the case for a Rae family of cratons. Precambrian Research 232, 27-43.

Peng, P., Zhai, M.G., Ernst, R.E., Guo, J.H., Liu, F., Hu, B., 2008. A 1.78 Ga large igneous province in the North China craton: the Xiong'er Volcanic Province and the North China dyke swarm. Lithos 101, 260-280.

Peng, T.P., Wilde, S.A., Fan, W.M., Peng, B.X., 2013. Neoarchean siliceous high-Mg basalt (SHMB) from the Taishan granite-greenstone terrane, Eastern North China Craton: petrogenesis and tectonic implications. Precambrian Research 228, 233-249.

Peng, P., Wang, C., Wang, X.P., Yang, S.Y., 2015. Qingyuan high-grade granite-greenstone terrain in the Eastern North China Craton: Root of a Neoarchaean arc. Tectonophysics 662, 7-21.

Piper, J.D.A., 2010. Protopangaea: Palaeomagnetic definition of Earth's oldest (mid-Archaean-Palaeoproterozoic) supercontinent. Journal of Geodynamics 50, 154-165.

Polat, A., Hofmann, A.W., Rosing, M.T., 2002. Boninite-like volcanic rocks in the 3.7-3.8 Ga Isua greenstone belt, West Greenland: geochemical evidence for intra-oceanic subduction zone processes in the early Earth. Chemical Geology 184, 231-254.

Polat, A., Hofmann, A.W., 2003. Alteration and geochemical patterns in the 3.7-3.8 Ga Isua greenstone belt, West Greenland. Precambrian Research 126, 197-218.

Polat, A., 2013. Geochemical variations in Archean volcanic rocks, southwestern Greenland: Traces of diverse tectonic settings in the early Earth. Geology 41, 379-380.

Qian, Q., Hermann, J., 2013. Partial melting of lower crust at 10-15 kbar: constraints on

adakite and TTG formation. Contributions to Mineralogy and Petrology 165, 1195-1224.

Rapp, R.P., Shimizu, N., Norman, M.D., Applegate, G.S., 1999. Reaction between slab-derived melts and peridotite in the mantle wedge: experimental constraints at 3.8 GPa. Chemical Geology 160, 335-356.

Reid, A., Jagodzinski, E.A., Fraser, G.L., Pawkey, M.J., 2014a. SHRIMP U–Pb zircon age constraints on the tectonics of the Neoarchean to early Paleoproterozoic transition within the Mulgathing Complex, Gawler Craton, South Australia. Precambrian Research 250, 27-49.

Reid, A., Jagodzinski, E.A., Armit, R.J., Dutch, R.A., Kirkland, C.L., Betts, P.G., Schaefer, B.F., 2014b. U-Pb and Hf isotopic evidence for Neoarchean and Paleoproterozoic basement in the buried northern Gawler Craton, South Australia. Precambrian Research 250, 127-142.

Reimink, J.R., Chacko, T., Stern, R.A., Heaman, L.M., 2014. Earth's earlist evolved crust generated in an Iceland-like setting. Nature Geoscience 7, 529-533.

Rollinson, H.R., 1993. Using geochemical data: evaluation, presentation, interpretation. Pearson Education Limited, London, pp, 108-111.

Ross, P.S., Bédard, J.H., 2009. Magmatic affinity of modern and ancient subalkaline volcanic rocks determined from trace-element discriminant diagrams. Canadian Journal of Earth Sciences 46, 823-839.

Samuel, V.O., Santosh, M., Liu, S.W., Wang, W., Sajeev, K., 2014. Neoarchean continental growth through arc magmatism in the Nilgiri Block, southern India. Precambrian Research 245, 146-173.

Santosh, M., Tsunogae, T., Li, J.H., Liu, S.J., 2007a. Discovery of sapphirine-bearing Mg-Al granulites in the North China Craton: implications for Paleoproterozoic ultrahigh temperature metamorphism. Gondwana Research 11, 263-285.

Santosh, M., Wilde, S.A., Li, J.H., 2007b. Timing of Paleoproterozoic ultrahigh-temperature metamorphism in the North China Craton: evidence from SHRIMP U-Pb zircon geochronology. Precambrian Research 159, 178-196.

Santosh, M., 2010. Assembling North China Craton within the Columbia supercontinent: the role of double-sided subduction. Precambrian Research 178, 149-167.

Santosh, M., Shaji, E., Tsunogae, T., Mohan, M.R., Satyanarayanan, M., Horie, K., 2013. Suprasubduction zone ophiolite from Agali hills: Petrology, zircon SHRIMP U-Pb geochronology, geochemistry and implications for Neoarchean plate tectonics in southern India. Precambrian Research 231, 301-324.

Santosh, M., Teng, X.M., He, X.F., Tang, Li., Yang, Q.Y., 2015. Discovery of Neoarchean suprasubduction zone ophiolite suite from Yishui Complex in the North China Craton. Gondwana Research, doi: 10.1016/j.gr.2015.10.017.

Sawyer, E.W., Cesare, B., Brown, M., 2011. When the continental crust melts. Elements 7, 229-233.

Schiano, P., Monzier, M., Eissen, J.P., Martin, H., Koga, K.T., 2010. Simple mixing as the major control of the evolution of volcanic suites in the Ecuadorian Andes. Contributions to Mineralogy and Petrology 160, 297-312.

Segal, I., Halicz, L., Platzner, I.T., 2003. Accurate isotope ratio measurements of ytterbium by multiple collection inductively coupled plasma mass spectrometry applying erbium and

hafnium in an improved double external normalization procedure. Journal of Analytical Atomic Spectrometry 18, 1217-1223.

Shan, H.X., Zhai, M.G., Oliveira, E.P., Santosh, M., Wang, F., 2015. Convergent margin magmatism and crustal evolution during Archean-Proterozoic transition in the Jiaobei terrane: Zircon U-Pb ages, geochemistry, and Nd isotopes of amphibolites and associated grey gneisses in the Jiaodong complex, North China Craton. Precambrian Research 264, 98-118.

Smithies, R.H., 2000. The Archean tonalite-trondhjemite-granodiorite (TTG) series is not an analogue of Cenozoic adakite. Earth and Planetary Science Letters 182, 115-125.

Soderlund, U., Patchett, P.J., Vervoort, J.D., Isachsen, C.E., 2004. The ^{176}Lu decay constant determined by Lu–Hf and U–Pb isotope systematics of Precambrian mafic intrusions. Earth and Planetary Science Letters 219, 311-324.

Song, B., Nutman, A.P., Liu, D.Y., Wu, J.S., 1996. 3800 to 2500 Ma crustal evolution in the Anshan area of Liaoning Province, northeastern China. Precambrian Research 78, 79-94.

Souza, Z.S., Martin, H., Peucat, J.J., Jardim de Sa, E.F., Macedo, M.H.F., 2007. Calc-alkaline magmatism at the Archean-Proterozoic transition: the Caico Complex Basement (NE Brazil). Journal of Petrology 48, 2149-2185.

Spencer, C.J., Cawood, P.A., Hawkesworth, C.J., Prave, A.R., Roberts, N.M.W., Horstwood, N.M.W., Horstwood, M.S.A., Whitehouse, M.J., EIMF. 2015. Generation and preservation of continental crust in the Grenville Orogeny. Geoscience Frontiers 6, 357-372.

Strand, K., Köykkä, J., 2012. Early Paleoproterozoic rift volcanism in the eastern Fennoscandian Shield related to the breakup of the Kenorland supercontinent. Precambrian Research 214-215, 95-105.

Streck, M.J., Leeman, W.P., Chesley, J., 2007. High-magnesian andesite from Mount Shasta: a product of magma mixing and contamination, not a primitive mantle melt. Geology 35, 351-354.

Sun, S.S., McDonough, W.F., 1989. Chemical and isotopic systematics of oceanic basalts: implications for mantle compositions and processes. In: Sauders, A.D., and Norry, M.J. (eds.), Magmatism in the Ocean Basins. Geological Society of London, Special Publication pp. 313-345.

Tang, L., Santosh, M., Teng, X.M., 2015. Paleoproterozoic (ca. 2.1-2.0 Ga) arc magmatism in the Fuping Complex: Implications for the tectonic evolution of the Trans-North China Orogen. Precambrian Research 268, 16-32.

Tang, L., Santosh, M., Tsunogae, T., Teng, X.M., 2016. Late Neoarchean arc magmatism and crustal growth associated with microblock amalgamation in the North China Craton: Evidence from the Fuping Complex. Lithos 248-251, 324-338.

van Achterbergh, E., Ryan, C., Jackson, S., Griffin, W.L., 2001. In: Sylvester, P. (Ed.), Appendix 3 Data Reduction Software for LA-ICP-MS in “Laser-Ablation-ICPMS in the Earth Sciences”: Mineralogical Association of Canada Short Course, vol. 29, pp. 239-243.

Wan, Y.S., Song, B., Geng, Y.S., Liu, D.Y., 2005a. Zircon SHRIMP U-Pb geochronology of Archean rocks from the Fushun-Qingyuan area, Liaoning Province and its geological

significance. Acta Geologica Sinica 79, 78-87 (in Chinese with English abstract).

Wan, Y.S., Song, B., Geng, Y.S., Liu, D.Y., 2005b. Geochemical characteristics of Archean basement in the Fushun-Qingyuan area, Northern Liaoning Province and its geological significance. Geological review 51, 128-137 (in Chinese with English abstract).

Wan, Y.S., Liu, D.Y., Dong, C.Y., Nutman, A., Wilde, S.A, Wang, W., Xie, H.Q., Yin, X.Y., Zhou, H.Y., 2009. The oldest rocks and zircons in China. Acta Petrologica Sinica 25, 1793-1807 (in Chinese with English abstract).

Wan, Y.S., Liu, D.Y., Wang, S.J., Dong, C.Y., Yang, E.X., Wang, W., Zhou, H.Y., Ning, Z.G., Du, L.L., Yin, X.Y., Xie, H.Q., Ma, M.Z., 2010. Juvenile magmatism and crustal recycling at the end of the Neoarchean in Western Shandong Province, North China Craton: evidence from SHRIMP zircon dating. American Journal of Science 310, 1503-1552.

Wan, Y.S., Dong, C.Y., Liu, D.Y., Kröner, A., Yang, C.H., Wang, W., Du, L.L., Xie, H.Q., Ma, M.Z., 2012. Zircon ages and geochemistry of late Neoarchean syenogranites in the North China Craton: A review. Precambrian Research 222-223, 265-289.

Wan, Y.S., Zhang, Y.H., Williams, I.S., Liu, D.Y., Dong, C.Y., Fan, R.L., Shi, Y.R., Ma, M.Z., 2013. Extreme zircon O isotopic compositions from 3.8 to 2.5 Ga magmatic rocks from the Anshan area, North China Craton. Chemical Geology 352, 108-124.

Wan, Y.S., Xie, S.W., Yang, C.H., Kröner, A., Ma, M.Z., Dong, C.Y., Du, L.L., Xie, H.Q., Liu, D.Y., 2014. Early Neoarchean (~2.7 Ga) tectono-thermal events in the North China Craton: A synthesis. Precambrian Research 247, 45-63.

Wan, Y.S., Ma, M.Z., Dong, C.Y., Xie, H.Q., Xie, S.W., Ren, P., Liu, D.Y., 2015. Widespread late Neoarchean reworking of Meso- to Paleoarchean continental crust in the

Anshan-Benxi area, North China Craton, as documented by U-Pb-Nd-Hf-O isotopes. American Journal of Science 315, 620-670.

Wang, S.S., Hu, S.L., Zhai, M.G., Sang, H.Q., Qiu, J., 1987. An application of the $^{40}Ar/^{39}Ar$ dating technique to the formation time of Qingyuan granite-greenstone terrain in NE China. Acta Geologica Sinica 4, 55-62 (in Chinese with English abstract).

Wang, Z.H., Wilde, S.A., Wang, K.Y., Yu, L.J., 2004. A MORB-arc basalt-adakite association in the 2.5 Ga Wutai greenstone belt: late Archean magmatism and crustal growth in the North China Craton. Precambrian Research 131, 323-343.

Wang, Y.J., Zhang, Y.Z., Zhao, G.C., Fan, W.M., Xia, X.P., Zhang, F.F., Zhang, A.M., 2009. Zircon U-Pb geochronological and geochemical constaints on the petrogenesis of the Taishan sanukitoids (Shandong): Implications for Neoarchean subduction in the Eastern Block, North China Craton. Precambrian Research 174, 273-286.

Wang, W., Liu, S.W., Bai, X., Yang, P.T., Li, Q.G., Zhang, L.F., 2011. Geochemistry and zircon U-Pb-Hf isotopic systematics of the Neoarchean Yixian-Fuxin greenstone belt, northern margin of the North China Craton: implications for petrogenesis and tectonic setting. Gondwana Research 20, 64-81.

Wang, W., Liu, S.W., Feng, Y.G., Li, Q.G., Wu, F.H., Wang, Z.Q., Wang, R.T., Yang, P.T., 2012a. Chronology, petrogenesis and tectonic setting of the Neoproterozoic Tongchang dioritic pluton at the northwestern margin of the Yangtze Block: Constraints from geochemistry and zircon U-Pb-Hf isotopic systematics. Gondwana Research 22, 699-716.

Wang, W., Liu, S.W., Wilde, S.A., Li, Q.G., Zhang, J., Bai, X., Yang, P.T., Guo, R.R., 2012b. Petrogenesis and geochronology of Precambrian granitoid gneisses in Western Liaoning

Province: Constraints on Neoarchean to early Paleoproterozoic crustal evolution of North China Craton. Precambrian Research 222-223, 290-311.

Wang, W., Liu, S.W., Bai, X., Li, Q.G., Yang, P.T., Zhao, Y., Zhang, S.H., Guo, R.R., 2013a. Geochemistry and zircon U-Pb-Hf isotopes of the late Paleoproterozoic Jianping diorite-monzonite-syenite suites of the North China Craton: implications for petrogenesis and geodynamic setting. Lithos 162-163, 175-194.

Wang, W., Liu, S.W., Santosh, M., Bai, X., Li, Q.G., Yang, P.T., Guo, R.R., 2013b. Zircon U-Pb-Hf isotopes and whole-rock geochemistry of granitoid gneisses in the Jianping gneissic terrane, Western Liaoning Province: constraints on the Neoarchean crustal evolution of the North China Craton. Precambrian Research 224, 184-221.

Wang, W., Liu, S.W., Santosh, M., Wang, G.H., Bai, X., Guo, R.R., 2015a. Neoarchean intra-oceanic arc system in the Western Liaoning Province: implications for the Early Precambrian crust-mantle geodynamic evolution of the Eastern Block of the North China Craton. Earth-Science Reviews 150, 329-364.

Wang, W., Liu, S.W., Santosh, M., Deng, Z.B., Guo, B.R., Zhao, Y., Zhang, S.H., Yang, P.T., Bai, X., Guo, R.R., 2015b. Late Paleoproterozoic geodynamics of the North China Craton: Geochemical and zircon U-Pb-Hf records from a volcanic suite in the Yanliao rift. Gondwana Research 27, 300-325.

Wang, W., Liu, S.W., Santosh, M., Zhang, L.F., Bai, X., Zhao, Y., Zhang, S.H., Guo, R.R., 2015c. 1.23 Ga mafic dykes in the North China Craton reconstruct the Columbia supercontinent. Gondwana Research 27, 1407-1418.

Wang, Y.F., Li, X.H., Jin, W., Zhang, J.H., 2015d. Eoarchean ultra-depleted mantle domains

inferred from ca. 3.8 Ga Anshan trondhjemitic gneisses, North China Craton. Precambrian Research 263, 88-107.

Wang, W., Liu, S.W., Bai, X., Guo, R.R., 2015e. Precambrian geodynamics (VIII): Late Archeean crustal growth models recorded in the North China Craton. Earth Science Frontiers 22, 109-124.

Winchester, J.A., Floyd, P.A., 1976. Geochemical magma type discrimination: application to altered and metamorphosed basic igneous rocks. Earth and Planetary Science Letters 28, 459-469.

Wu, F.Y., Yang, Y.H., Xie, L.W., Yang, J.H., Xu, P., 2006. Hf isotopic compositions of the standard zircons and baddeleyites used in U-Pb geochronology. Chemical Geology 234, 105-126.

Wu, M.L., Zhao, G.C., Sun, M., Li, S.Z., He, Y.H., Bao, Z.A., 2013a. Zircon U-Pb geochronology and Hf isotopes of major lithologies from the Yishui Terrane: Implications for the crustal evolution of the Eastern Block, North China Craton. Lithos 170-171, 164-178.

Wu, K.K., Zhao, G.C., Sun, M., Yin, C.Q., He, Y.H., Pui, Y.T., 2013b. Metamorphism of the northern Liaoning Complex: implications for the tectonic evolution of Neoarchean basement of the Eastern Block, North China Craton. Geoscience Frontiers 4, 305-320.

Wu, M.L., 2014. Ages, geochemistry and metamorphism of Neoarchean basement in Shandong Province. Springer-Verlag, New York, pp. 1-243.

Wu, M.L., Zhao, G.C., Sun, M., Li, S.Z., Bao, Z.A., Tam, P.Y., Eizenhöefer, P.R., He, Y.H., 2014. Zircon U-Pb geochronology and Hf isotopes of major lithologies from the Jiaodong

Terrane: Implications for the crustal evolution of the Eastern Block of the North China Craton. Lithos 190-191, 71-84.

Wu, M.L., Lin, S.F., Wan, Y.S., Gao, J.F., 2016. Crustal evolution of the Eastern Block in the North China Craton: constraints from zircon U-Pb geochronology and Lu-Hf isotopes of the North Liaoning Complex. Precambrian Research 275, 35-47.

Yang, J.H., Wu, F.Y., Wilde, S.A., Zhao, G.C., 2008. Petrogenesis and geodynamics of Late Archean magmatism in eastern Hebei, eastern North China Craton: Geochronological, geochemical and Nd–Hf isotopic evidence. Precambrian Research 167, 125-149.

Yang, Q.Y., Santosh, M., Pradeepkumar, A.P., Shaji, E., Prasanth, R.S., Dhanil Dev, S.G., 2015. Crustal evolution in the western margin of the Nilgiri Block, southern India: Insights from zircon U–Pb and Lu–Hf data on Neoarchean magmatic suite. Journal of Asian Earth Sciences, doi:10.1016/j.jseaes.2015.02.023.

Yuan, H.L., Gao, S., Liu, X.M., Li, H.M., Günther, D., Wu, F.Y., 2004. Accurate U-Pb age and trace element determinations of zircon by laser ablation inductively coupled plasma-mass spectrometry. Geostandard and Geoanalytical Research 28, 353-370.

Zamora, D., 2000. Fusion de la croute oceanique subductee: approche experimentale et geochimique. Universite Thesis Universite Blaise Pascal, Clermont-Ferrand, pp. 314.

Zhai, M.G., Yang, R.Y., Lu, W.J., Zhou, J.E., 1985. Geochemistry and evolution of the Qingyuan Archaean granite-greenstone terrain, NE China. Precambrian Research 27, 37-62.

Zhai, M.G., Santosh, M., 2011. The Early Precambrian odyssey of the North China Craton: a synoptic overview. Gondwana Research 20, 6-25.

Zhai, M.G., Santosh, M., 2013. Metallogeny of the North China Craton: Link with secular changes in the evolving Earth. Gondwana Research 24, 275-297.

Zhai, M.G., Hu, B., Zhao, T.P., Peng, P., Meng, Q.R., 2015. Late Paleoproterozoic-Neoproterozoic multi-rifting events in the North China Craton and their geological significance: A study advance and review. Tectonophysics, 662, 153-166.

Zhang, X.H., Yuan, L.L., Xue, F.H., Zhang, Y.B., 2012. Contrasting Triassic ferroan granitoids from northwestern Liaoning, North China: magmatic monitor of Mesozoic decratonization and a craton-orogen boundary. Lithos 144-145, 12-23.

Zhang, Z.M., Dong, X., Xiang, H., Liou, J.G., Santosh, M., 2013a. Building of the deep Gangdese arc, SouthTibet: Paleocene plutonism and granulite-facies metamorphism. Journal of Petrology 54, 2547-2580.

Zhang, J.X., Yu, S.Y., Gong, J.H., Li, H.K., Hou, K.J., 2013b. The latest Neoarchean-Paleoproterozoic evolution of the Dunhuang block, eastern Tarim craton, northwestern China: evidence from zircon U-Pb dating and Hf isotopic analyses. Precambrian Research 226, 21-42.

Zhang, X.H., Yuan, L.L., Wilde, S.A., 2014. Crust/mantle interaction during the construction of an extensional magmatic dome: middle to late Jurassic plutonic complex from western Liaoning, North China Craton. Lithos 205, 185-207.

Zhao, G, C., Wilde, S.A., Cawood, P.A., Lu, L.Z., 1998. Thermal evolution of Archean basement rocks from the eastern part of the North China carton and its bearing on tectonic setting. International Geology Review 40, 706-721.

Zhao, G.C., Sun, M., Wilde, S.A., 2003. Correlations between the Eastern Block of the North

China Craton and the South Indian Block of the Indian Shield: an Archean to Paleoproterozoic link. Precambrian Research 122, 201-233.

Zhao, G.C., Sun, M., Wilde, S.A., Li, S.Z., 2004. A Paleo-Mesoproterozoic supercontinent: assembly, growth and breakup. Earth-Science Reviews 67, 91-123.

Zhao, G.C., Sun, M.,Wilde, S.A., Li, S.Z., 2005. Late Archean to proterozoic evolution of the North China Craton: Key issues revisited. Precambrian Research 136, 177-202.

Zhao, G.C., Cawood, P.A., Li, S.Z., Wilde, S.A., Sun, M., Zhang, J., He, Y.H., Yin, C.Q., 2012. Amalgamation of the North China Craton: key issues and discussions. Precambrian Research 222-223, 55-76.

Zhu, M.T., Zhang, L.C., Dai, Y.P., Wang, C.L., 2015. In situ zircon U-Pb dating and O isotopes of the Neoarchean Hongtoushan VMS Cu-Zn deposit in the North China Craton: Implication for the ore genesis. Ore Geology Reviews 67, 354-367.

Figure Captions:

Fig. 1. (A) Geological sketch map of the North China Craton (NCC) illustrating major early Precambrian basement terranes and late Paleoproterozoic tectonic framework (modified from Zhao et al. (2005, 2012) and Santosh (2010)). Archean crystalline basement of the Northern Liaoning Province (NLP of Fig. 2) is shown by the rectangle. (B) Archean crust-mantle geodynamic model for the Eastern Block (EB) proposed by Wang et al. (2015a). A large ~2.6-2.5 Ga intra-oceanic arc system was proposed along the northwestern margin of the EB, marking a major late Neoarchean crustal growth episode related to arc-continent accretion. The spatial distribution scopes of early Neoarchean and pre-Neoarchean basement terranes

within the EB were also delineated. Abbreviations: CD-Chengde; DF-Dengfeng; EH-Eastern Hebei; FP-Fuping; HA-Huai'an; HS-Hengshan; JD-Jiaodong; LL-Lvliang; NH-Northern Hebei; NL-Northern Liaoning; SJ-Southern Jilin; SL-Southern Liaoning; TH-Taihua; WL-Western Liaoning; WT-Wutai; WS-Western Shandong; XH-Xuanhua; ZH-Zanhuang; ZT-Zhongtiao.

Fig. 2. (A) Simplified geological map of the NLP showing major lithological units and the Hunhe Fault, with the Qingyuan area (Fig. 2B) along the northeastern NLP marked by the rectangle. (B) Detailed geological map of the northeastern NLP showing regional geological setting and sampling locations (dated samples are marked by the blue stars).

Fig. 3. Field photographs for Archean crystalline basement in the Qingyuan area of the northeastern NLP, showing (A) interlayered metamorphosed supracrustal rocks of mafic granulites, (garnet) amphibolites, hornblende plagioclase gneisses, and biotite plagioclase gneisses, along with some metasedimentary rocks (e.g., BIFs and clastic sedimentary rocks). The scale bar is 1m long; (B-C) trondhjemitic and tonalitic gneisses with strong gneissosity. The student and the card are ~1.8 m high and ~10 cm long, respectively; (D) xenoliths of metavolcanic rocks within tonalitic gneisses; (E-F) weakly gneissic to massive quartz monzodioritic and monzogranitic gneisses, the hammer is ~30 cm long; (G) weakly gneissic monzogranitic veins crosscutting tonalitic gneisses; and (H) amphibolitic gneisses with a rectangle shape within quartz monzodioritic gneisses.

Fig. 4. Photomicrographs for representative late Neoarchean granitoid gneisses in the

Qingyuan area: (A) biotite hornblende plagioclase gneiss (quartz dioritic gneiss sample 12LN75-2); (B) biotite plagioclase gneiss (tonalitic gneiss sample 13LB37-3); (C) hornblende two pyroxene granulite (tonalitic gneiss sample 13LB32-5); (D) (hornblende) biotite plagioclase gneiss (trondhjemitic gneiss sample 12LN78-1); (E) quartz monzodirotic granulitic gneiss sample 13LB33-3; and (F) biotite two feldspar gneiss (monzogranitic gneiss sample 13LB31-1). Mineral abbreviations: Cpx-clinopyroxene; Opx-orthopyroxene; Hb-hornblende; Bt-biotite; Pl-plagioclase; Kfs-potassic feldspar; Qz-quartz.

Fig. 5. Major element compositions of late Neoarchean granitoid gneisses in the Qingyuan area: (A) An-Ab-Or diagram (O'Connor, 1965); (B) K_2O-Na_2O-CaO diagram, showing a sodium-rich trend (the DTT series of trend (1)) and a potassium-rich trend (the MM series of trend (2)) (Moyen et al., 2003); (C) K_2O versus SiO_2 diagram (Rollinson, 1993); and (D) MgO versus SiO_2 diagram (PMB: experimentally-derived partial melts from metabasaltic rocks; LSA-low silica adakite; HSA-high silica adakite, after Martin et al. (2005)). Symbols: solid squares-quartz dioritic gneisses; open diamonds-tonalitic to trondhjemitic gneisses; solid circles-quartz monzodioritic gneisses of this study; open circles-quartz monzodioritic gneisses in Xinbin reported by Peng et al. (2015); cross-monzogranitic gneisses.

Fig. 6. Chondrite-normalized REE patterns and primitive mantle-normalized multi-element patterns for (A-B) quartz dioritic gneisses; (C-D) tonalitic and trondhjemitic gneisses; (E-F) quartz monzodioritic gneisses; and (G-H) monzogranitic gneisses (samples north of the Qingyuan county and north of Nanzamu town are designated separately). Symbols are the

same as Fig. 5, and chondrite and primitive mantle values after Sun and McDonough (1989).

Fig. 7. Cathodoluminescence images for zircons from trondhjemitic gneiss samples 12LN78-1 (A) and 13LB47-3 (B); tonalitic gneiss sample 13LB46-5 (C); trondhjemitic gneiss sample 13LB26-5 (D); and monzogranitic gneiss samples 12LN59-1 (E) and 12LN80-1 (F), showing internal structures, analytical domains for both zircon U-Pb (small circles with solid line) and Lu-Hf (large circles with dashed line) isotopic data, apparent $^{207}Pb/^{206}Pb$ ages, and $\varepsilon Hf(t_2)$ values calculated at the crystallization age (t_2). Numbers are analyzed sample locations.

Fig. 8. Concordia diagrams showing LA-ICPMS zircon U-Pb isotopic dating data and calculated ages for representative late Neoarchean granitoid gneiss samples in Qingyuan area: (A) 12LN78-1, (B) 13LB47-3, (C) 13LB46-5, (D) 13LB26-5, (E) 12LN59-1, and (F) 12LN80-1.

Fig. 9. Zircon $\varepsilon Hf(t_2)$ values versus crystallization ages (t_2) for samples in the Qingyuan area (A) and their comparisons to zircon Lu-Hf isotopic data of early Archean lithological units in the adjoining Anshan-Benxi terrane (B). Lu-Hf isotopic data of the captured zircon grains are calculated at the $^{207}Pb/^{206}Pb$ ages (t_1), whereas the other spots are calculated at the magmatic crystallization ages of each sample (t_2). $^{176}Lu/^{177}Hf$ ratios of depleted mantle and chondrite are 0.0384 and 0.0332, respectively (Blichert-Toft and Albarède, 1997; Griffin et al., 2000).

Fig. 10. Summary of major early Precambrian tectonothermal events in the NLP (see detailed chronological data in Supplementary Table 4). (A) Histogram of major magmatic events,

showing the formation of supracrustal metavolcanic rocks at ~2570 Ma and ~2530 Ma, TTG gneisses at ~2559-2503 Ma, and potassium-rich granitoid gneisses at ~2529-2496 Ma, respectively. (B) Histogram of major metamorphic events, showing ~2510-2495 Ma peak high-grade metamorphism and later multi-stage retrograde metamorphism at ~2479-2461 Ma, ~2427 Ma, and ~2350 Ma. Emplacement of potassium-rich granitoid rocks was nearly coeval with the high-grade metamorphism. (C) Histogram showing age patterns of xenocrystic or inherited zircon grains, with major age populations at middle to late Neoarchean (2674 ± 48 Ma - 2553 ± 26 Ma), but only minor at ~3.1 Ga and ~2.7 Ga.

Fig. 11. Petrogenetic diagrams for quartz dioritic and tonalitic to trondhjemitic gneisses of the DTT series, indicating their derivation from partial melting of descending slabs (quartz dioritic gneisses) and lower arc crustal materials (tonalitic to trondhjemitic gneisses), respectively. (A) $(La/Yb)_N$ versus $(La)_N$ diagram, discriminating adakitic rocks and subduction-related calc-alkaline basalitic-andesitic-dacitic-rhyolitic rocks (Martin, 1986). (B) Mg# ($100Mg/(Mg+Fe_{total})$ atomic ratio) versus SiO_2 diagram (reference fields for hybridised melts at 4 GPa, sanukitoids and experimental melts at 1-4 GPa are from Souza et al. (2007) and references therein, and that for adakites after Smithies (2000)). (C) Dy/Yb versus SiO_2 diagram (Wang et al., 2015a). With increasing SiO_2 contents, the tonalitic to trondhjemitic gneisses show a increase in Dy/Yb ratios. (D) Molar $Al_2O_3/(MgO+FeO_T)$ (AFM) versus molar $CaO/(MgO+FeO_T)$ (CFM) diagram showing source compositions for the granitoid gneisses (modified from Altherr et al. (2000)). (E) Nb versus Y diagram (Pearce, 1984), discriminating different groups of TTG gneisses (i.e., high/medium/low-pressure types after Moyen (2011)).

WPG-within plate granites; ORG-ocean ridge granites; VAG-volcanic arc granites; Syn-COLG-syn-collisional granites. (F) Nb/Ta versus Zr/Sm diagram after Foley et al. (2002). Granitoid rocks with distinct Nb/Ta ratios may be derived from partial melting of metabasaltic rocks under diverse pressures (rutile eclogites/rutile-free eclogites/amphibolites). The horizontal and vertical lines represent chondritic Nb/Ta and Zr/Sm ratios of 17.6 and 25, respectively.

Fig. 12. Petrogenetic diagrams for quartz monzodioritic and monzogranitic gneisses of the MM series, suggesting their derivation dominantly from partial melting of depleted mantle source metasomatized chiefly by slab-derived fluids and of metagreywackes, respectively. (A) $(La/Yb)_N$ versus $(La)_N$ diagram (Martin, 1986). (B) La versus La/V diagram. The inset is a schematic C^I versus C^I/C^C diagram (I and C being incompatible and compatible elements, respectively) with curves showing compositions produced by magma mixing, fractional crystallization and partial melting (Schiano et al. (2010)). (C) $(Hf/Sm)_N$ versus $(Nb/La)_N$ diagram (LaFlèche et al., 1998). (D) CaO/Al_2O_3 versus SiO_2 diagram, illustrating the effects of clinopyroxene (Cpx) fractionation. (E) Dy/Yb versus MgO diagram (Wang et al., 2015a), with quartz monzodioritic gneiss samples showing similar Dy/Yb ratios. (F) AFM versus CFM diagram, showing source compositions of the monzogranitic gneiss samples.

Fig. 13. Geochemical features and petrogenetic discrimination diagrams for supracrustal metamorphosed basaltic to andesitic rocks in the Northern Liaoning Province (Wan et al., 2005a). (A) Zr/TiO_2*0.0001 versus Nb/Y diagram (Winchester and Floyd, 1977). (B) La versus

Yb diagram (Ross and Bédard, 2009). (C) $(Nb/La)_{PM}$ versus $(La/Sm)_N$ diagram (Sun and McDonough, 1989). (D) La/Yb versus Nb/Yb diagram; shaded area represents parental magmas derived from mantle sources not metasomatized by slab-derived fluids or melts (i.e., N-MORB, E-MORB, and OIB, related parameters of which after Sun and McDonough (1989)).

Fig. 14. Late Neoarchean crust-mantle geodynamic evolution model of the Northern Liaoning Province, showing transition from mid-ocean ridge spreading, through initiation and maturation of an intra-oceanic arc system, to arc-continent accretion. (A) Neoarchean mid-ocean ridge magmatism at or prior to ~2570 Ma, generating N-MORB-like basaltic rocks; (B) Incipient subduction of oceanic slabs and evolution of an intra-oceanic arc system, forming dominantly calc-alkaline and subordinate tholeiitic basalts (~2570 Ma); (C) With the maturation of the intra-oceanic arc system at ~2550-2530 Ma, partial melting of descending oceanic slabs and lower arc crustal materials, respectively led to the generation of quartz dioritic and tonalitic to trondhjemitic plutonic rocks of the DTT series; (D) During ~2520-2490 Ma, the accretion of the arc system to the northern margin of the EB possibly triggered slab rollback processes. Upwelling of hot asthenospheric mantle induced partial melting of the depleted lithospheric mantle and both juvenile arc crust and ancient continental margin materials, leading to the production of dominantly quartz monzodioritic and monzogranitic rocks of the MM series.

Supplementary Fig. 1. Covariation diagrams of Zr versus representative (A–B) LREEs (La and Sm), (C) HFSEs (Nb), and (D-F) LILEs (Th, Ba, and Rb) for the late Neoarchean granitoid gneisses in the Qingyuan area. The general positive correlations between Zr and La, Sm, and

Nb indicate that the primary igneous LREE and HFSE contents are generally preserved. The large scatters of Th, Ba, and Rb suggest that these LILEs have been mobilized, and cannot be used for petrogenetic discussions.

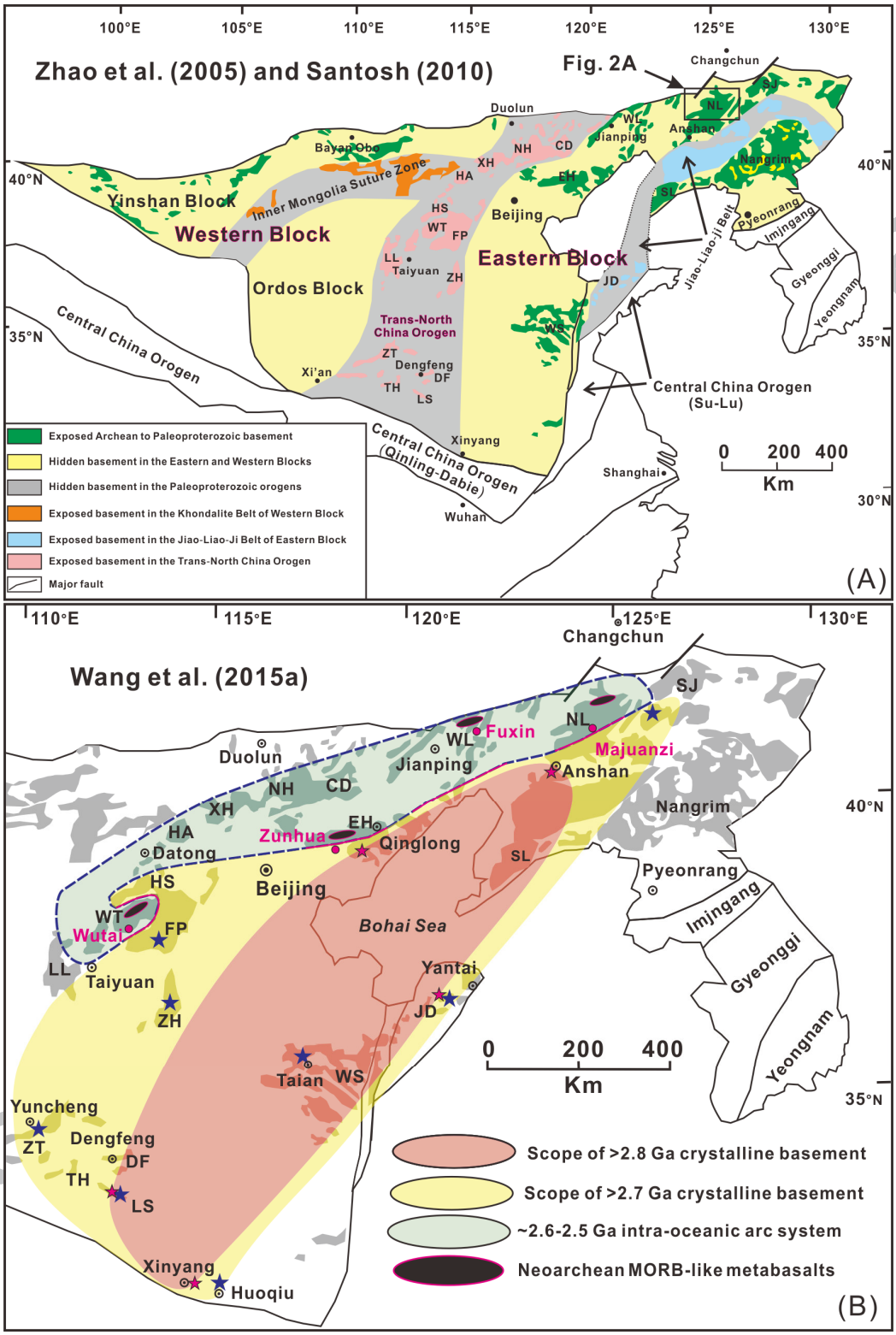

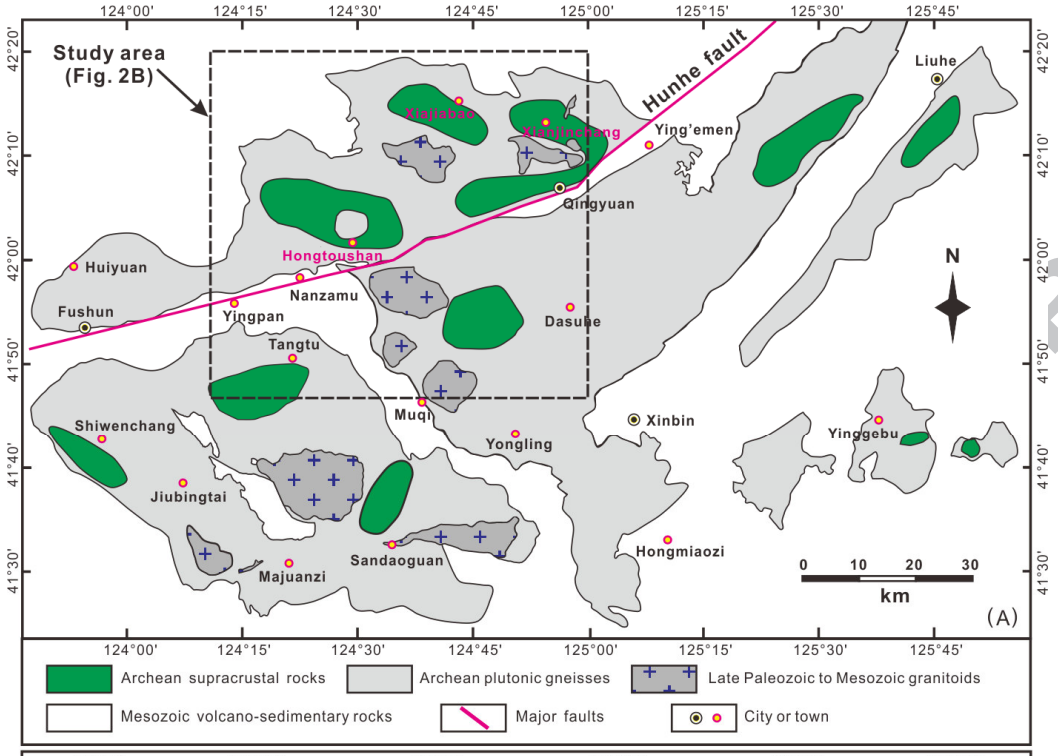

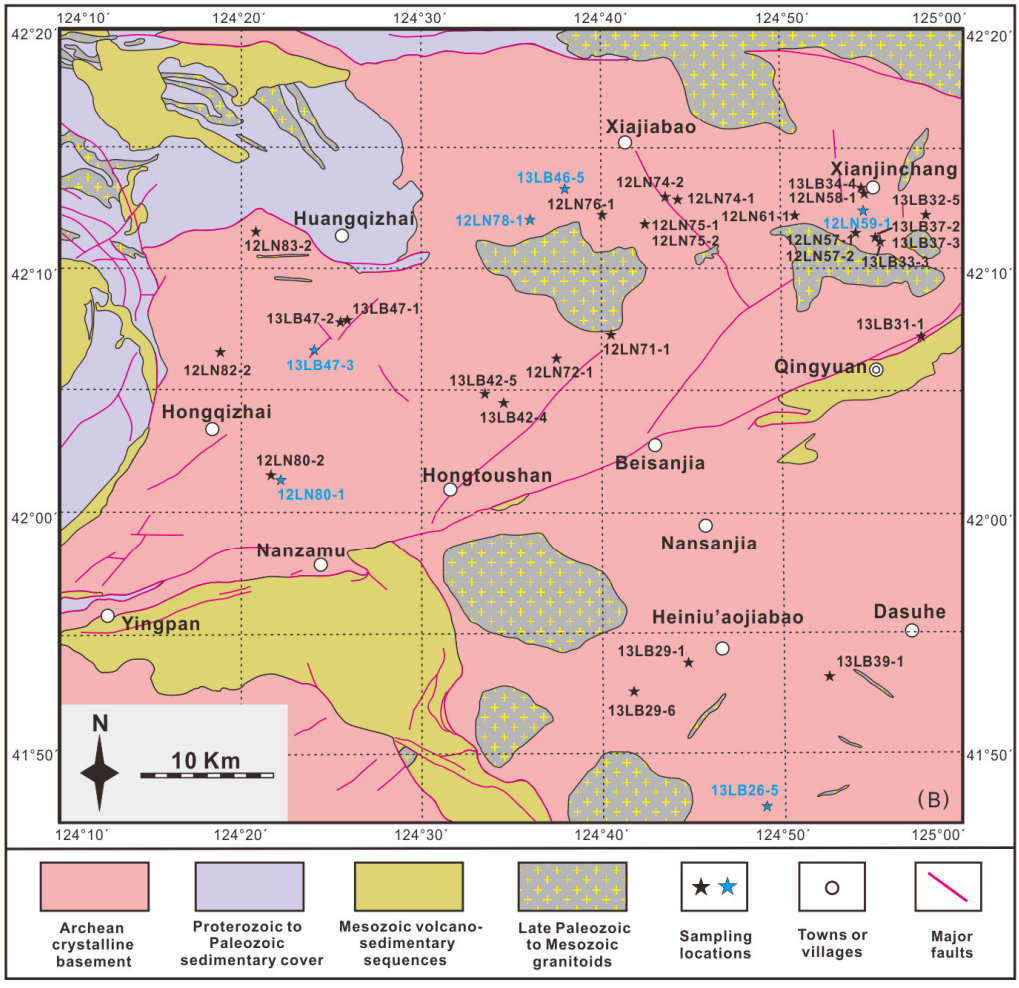

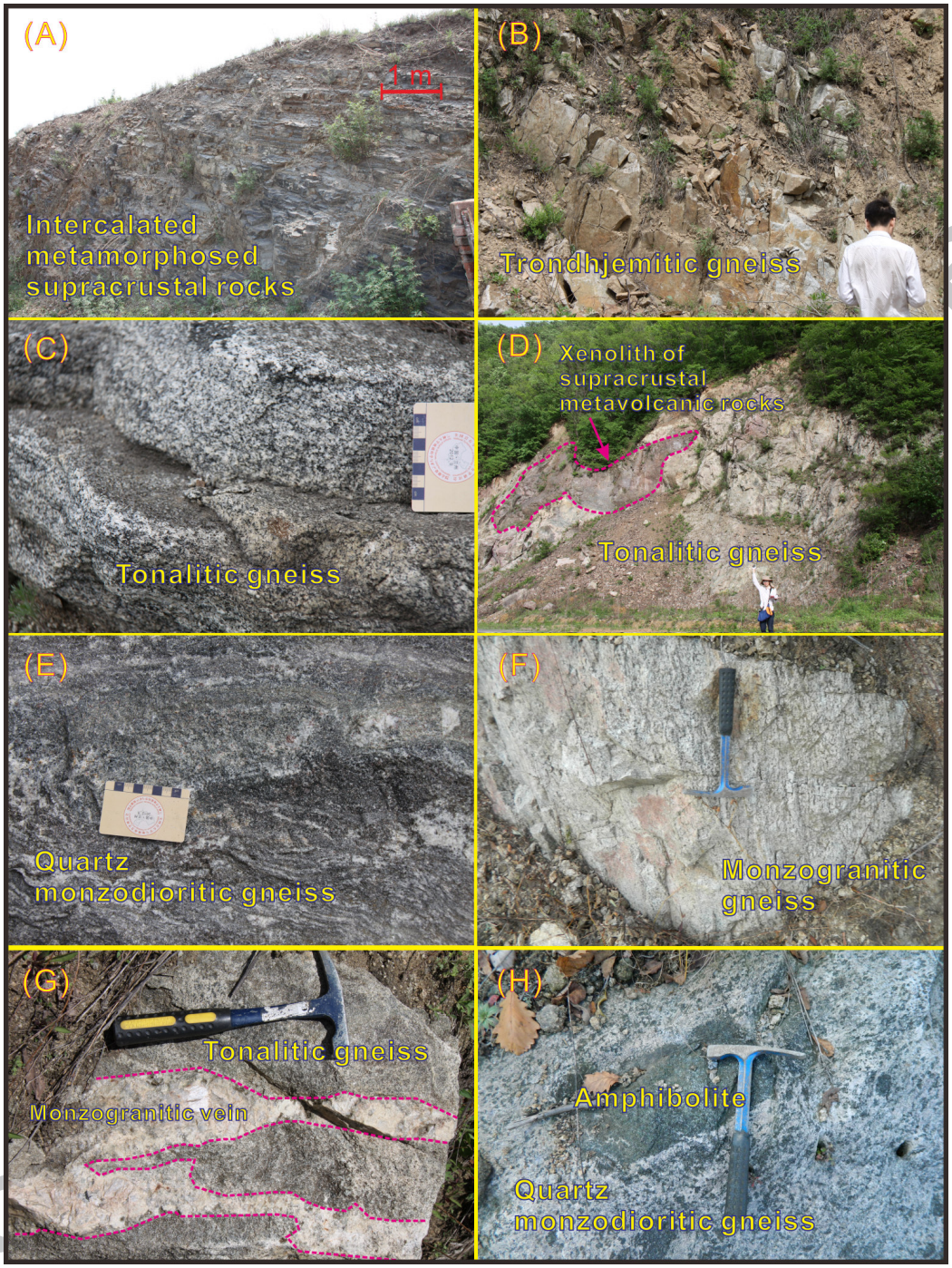

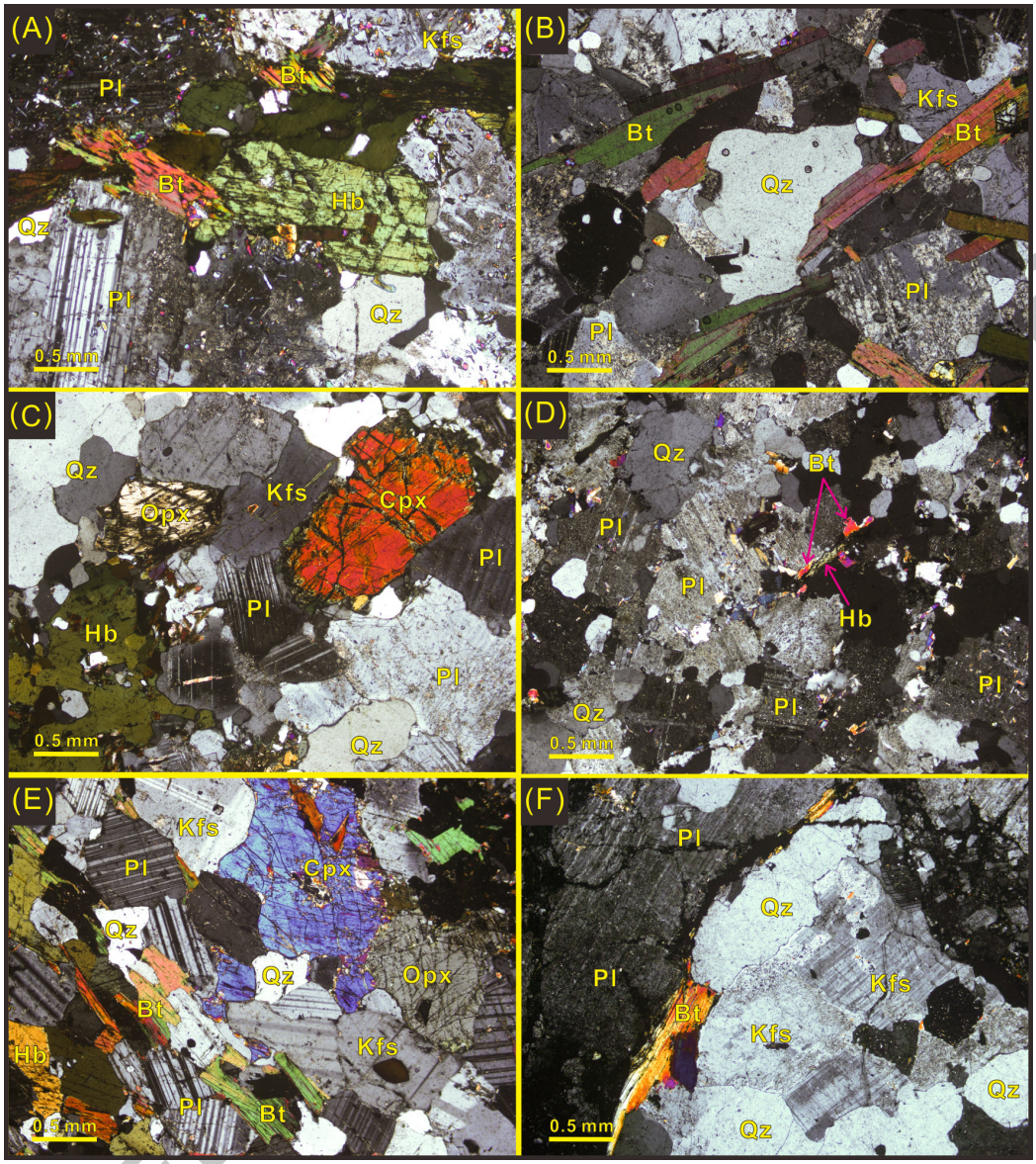

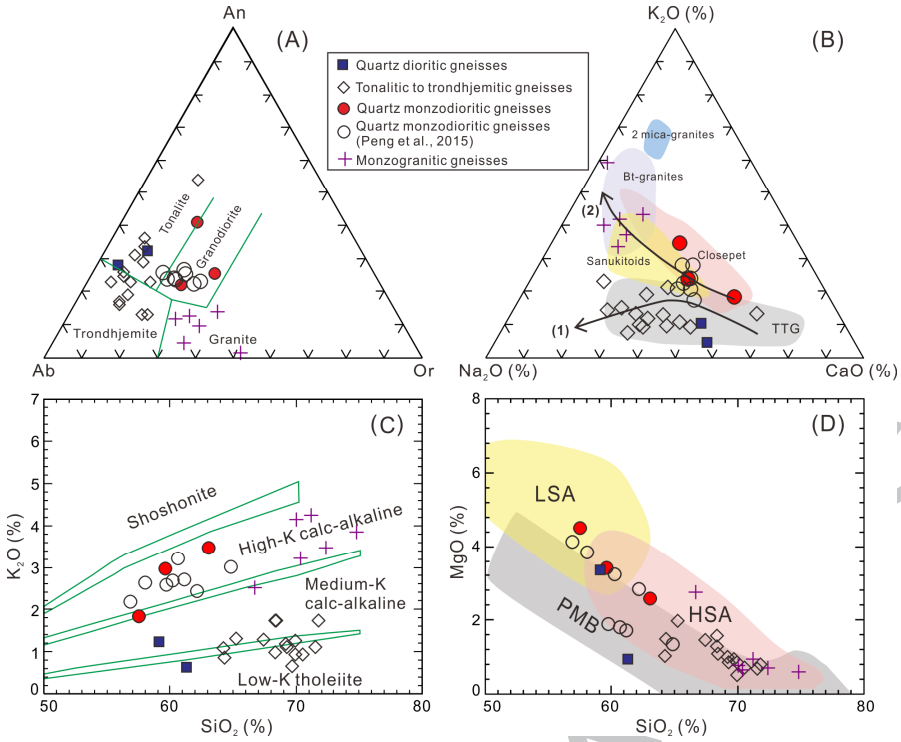

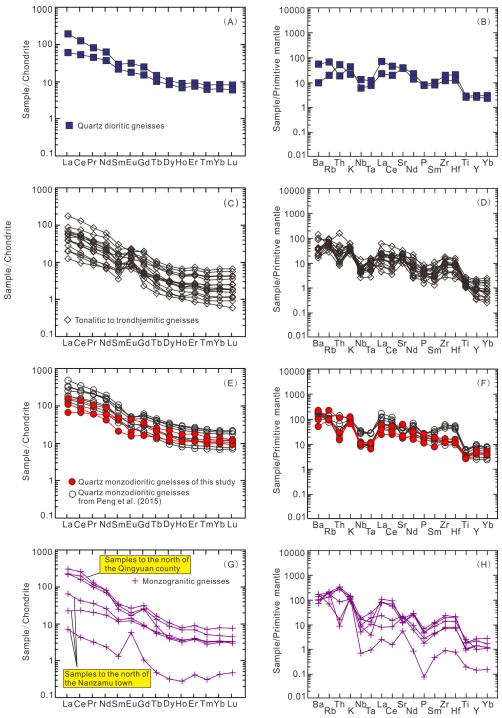

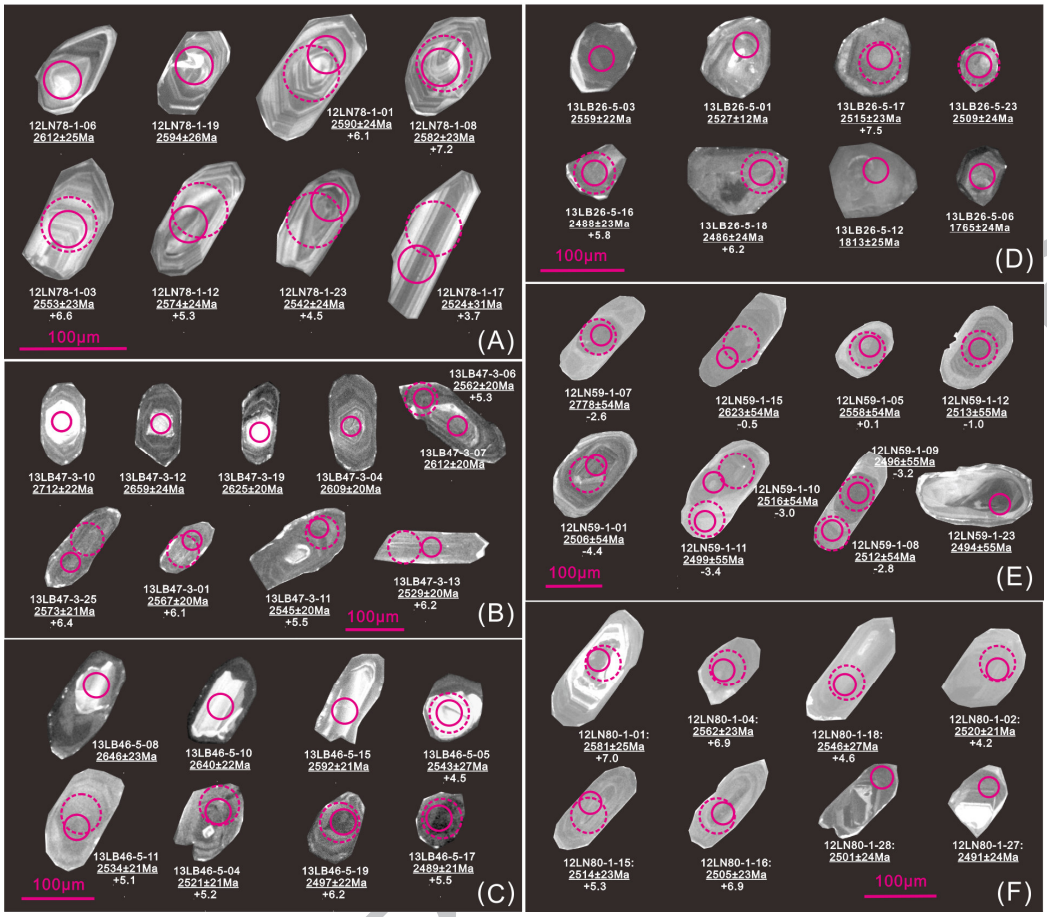

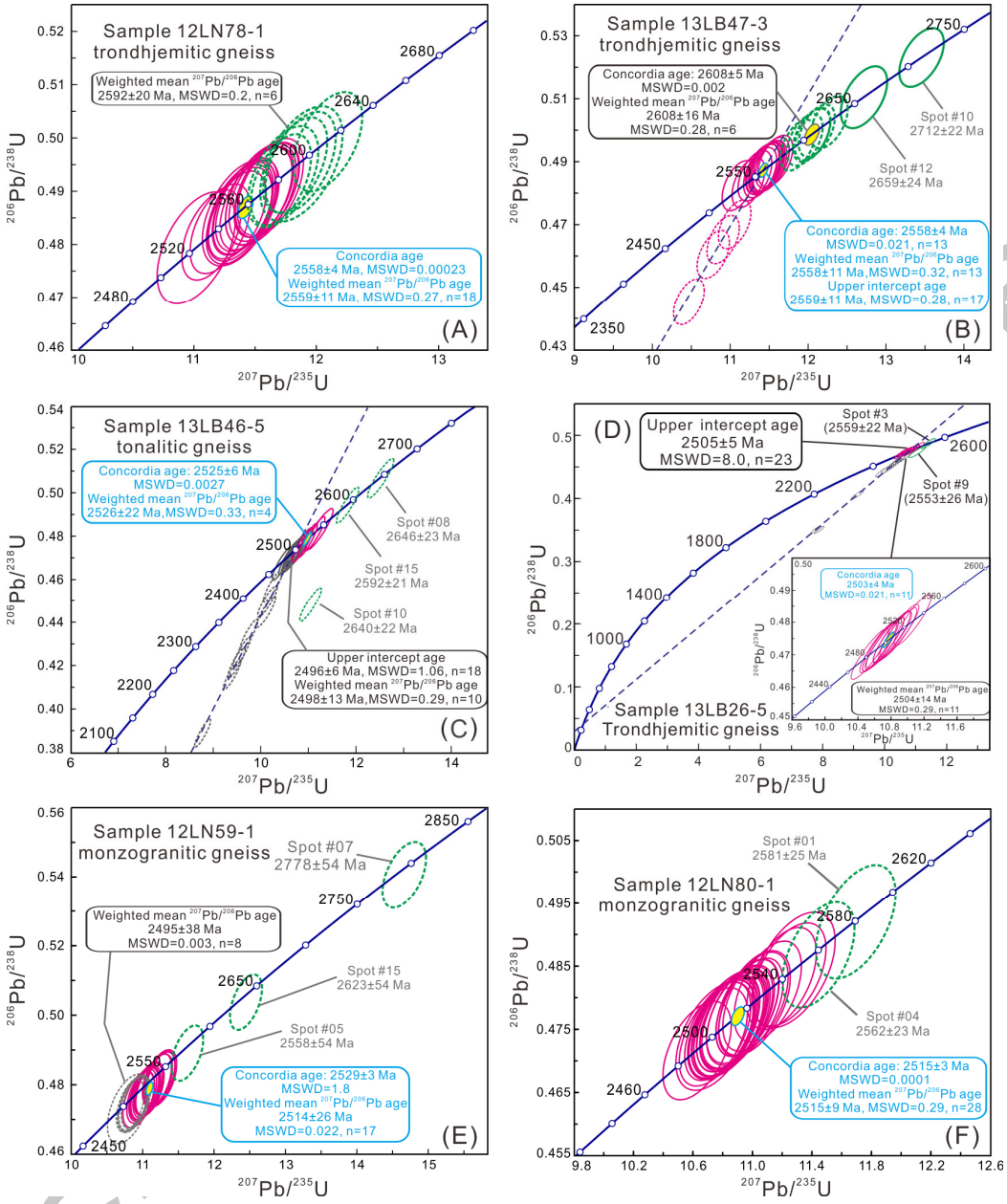

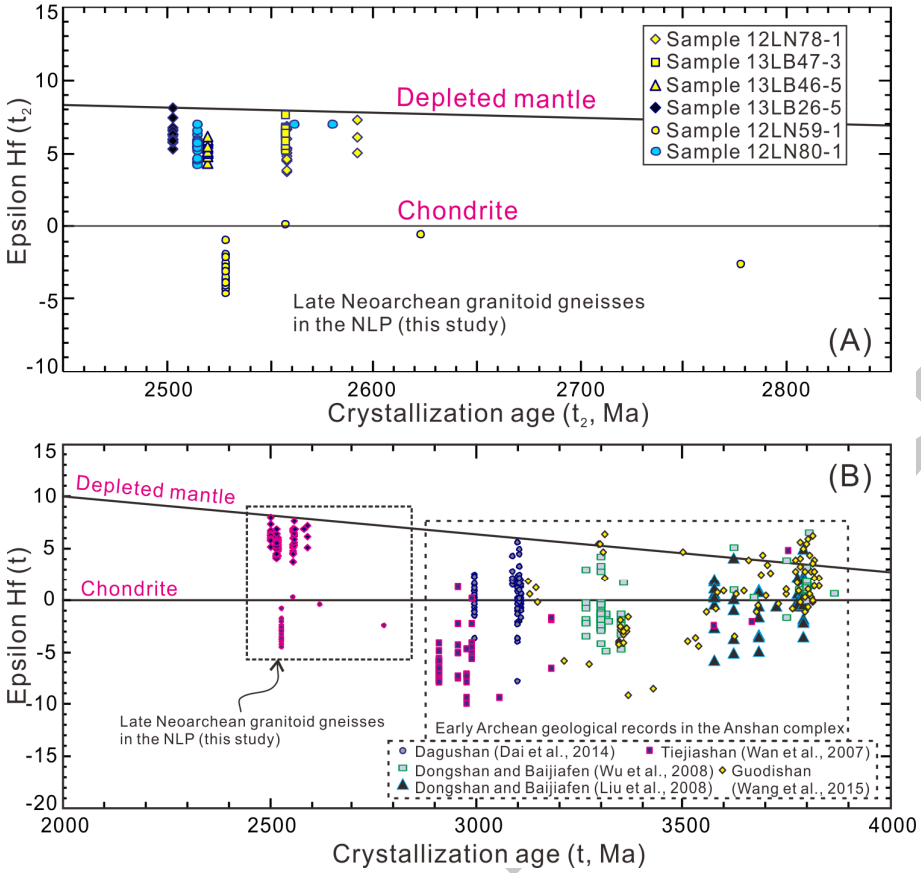

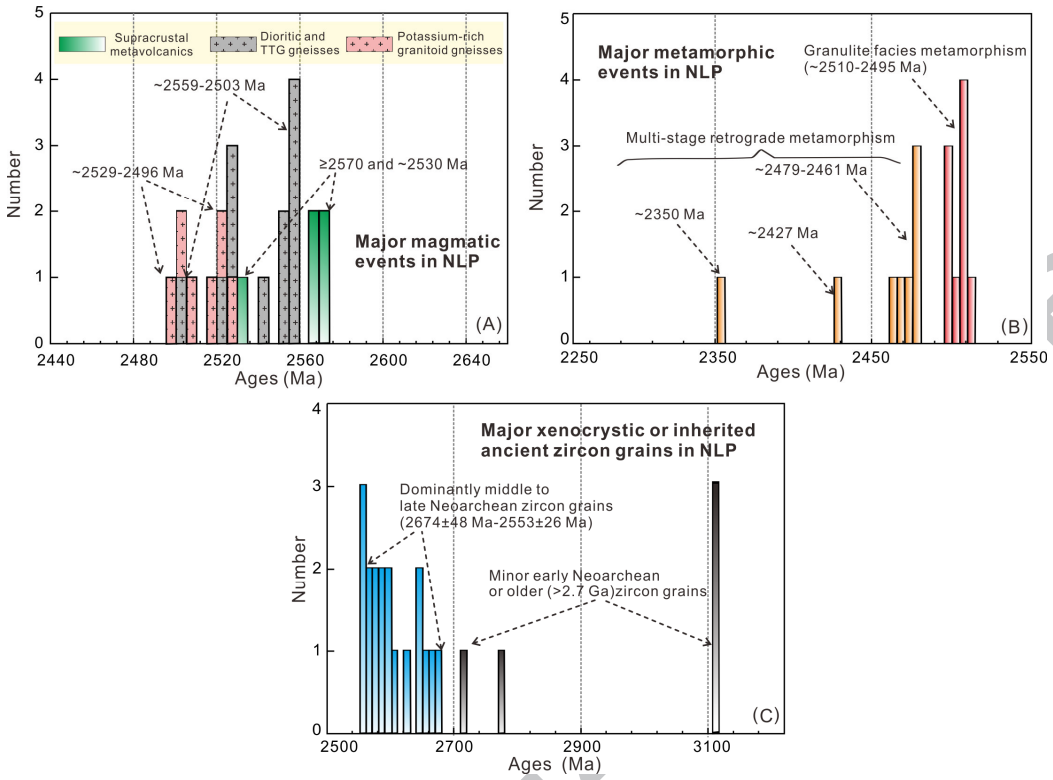

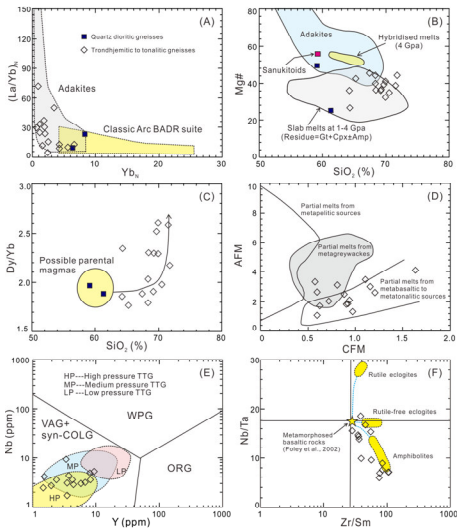

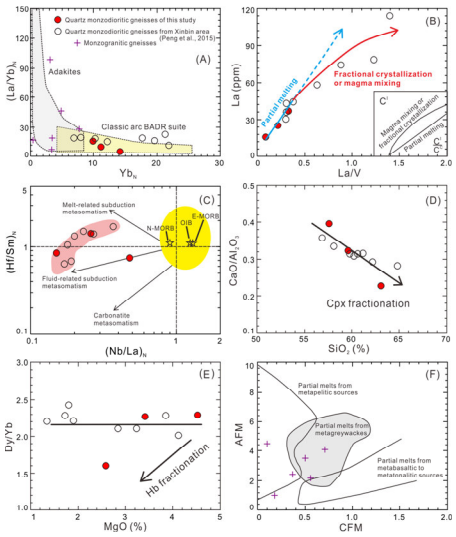

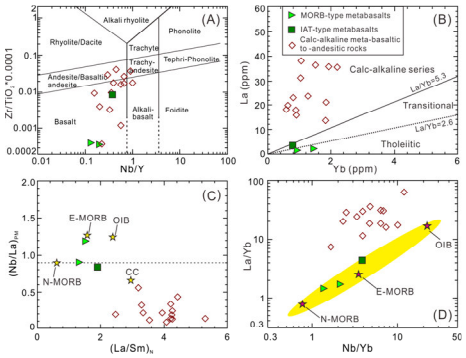

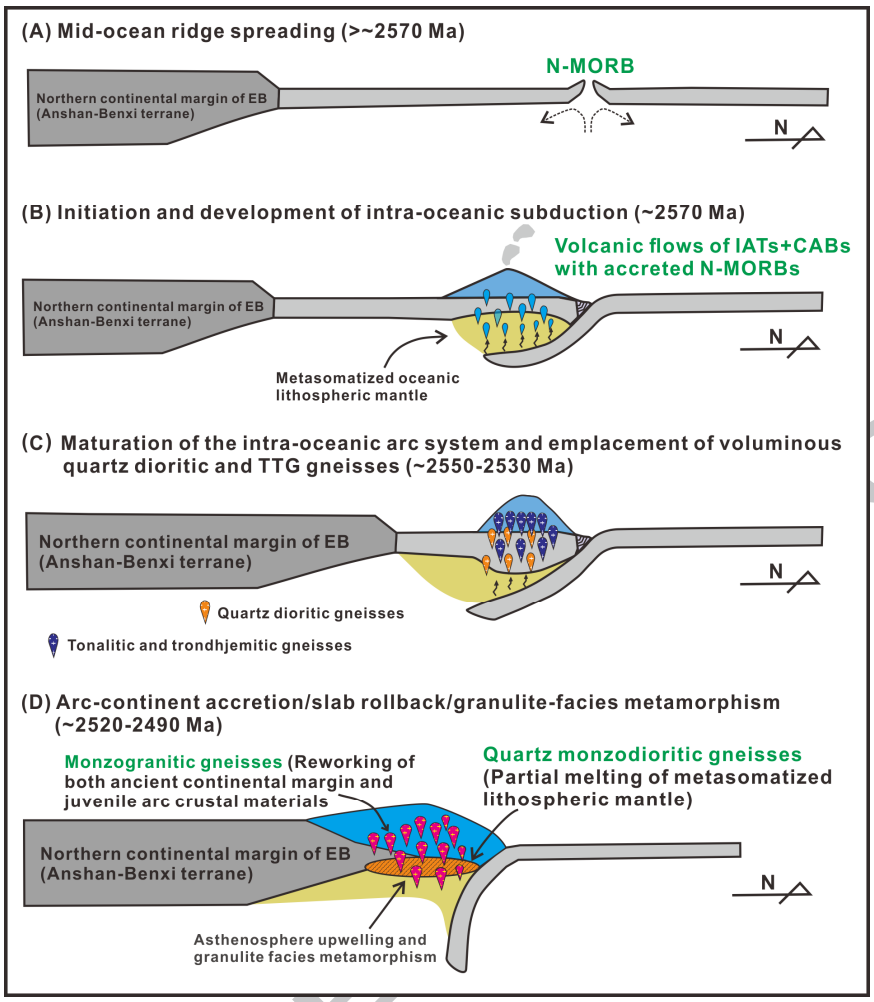

Research Highlights:

- Voluminous ~2559-2495 Ma granitoid gneisses in Northern Liaoning, NCC;
- Quartz dioritic to TTG gneisses stemmed from juvenile basaltic rocks;
- Potassium-rich granitoids sourced from metasomatized mantle or metagreywackes;
- A late Neoarchean (~2.6-2.5 Ga) arc-continent accretion system;
- Significant late Neoarchean crustal growth of the NLP and the entire NCC.

Late Neoarchean quartz dioritic, tonalitic, trondhjemitic, and potassium-rich granitoid gneisses recording arc-continent accretion-related crustal growth in the Northern Liaoning Province, North China Craton